JGR Atmospheres

RESEARCH ARTICLE
10.1029/2019JD032117

On the Relationship Between the Madden-Julian Oscillation and the Hadley and Walker Circulations

Juliane Schwendike[1], Gareth J. Berry[1], Katherine Fodor[1,2], and Michael J. Reeder[3]

[1]School of Earth and Environment, University of Leeds, Leeds, UK, [2]Max-Planck Institut für Meteorologie, Hamburg, Germany, [3]School of Earth, Atmosphere and Environment and the ARC Centre of Excellence for Climate Extremes, Monash University, Melbourne, Victoria, Australia

Key Points:

- Regional Hadley circulation is strengthened during active phase of the Madden-Julian Oscillation (MJO)
- Walker circulation in Pacific Ocean doubles in strength when MJO convection is over Maritime Continent
- Subtropical jet is strengthened and displaced further poleward in regions of enhanced convection

Correspondence to:
J. Schwendike,
j.schwendike@leeds.ac.uk

Citation:
Schwendike, J., Berry, G. J., Fodor, K., & Reeder, M. J. (2021). On the relationship between the Madden-Julian Oscillation and the Hadley and Walker circulations. *Journal of Geophysical Research: Atmospheres*, *126*. https://doi.org/10.1029/2019JD032117

Received 24 NOV 2019
Accepted 3 JAN 2021

Author Contributions:
Conceptualization: Juliane Schwendike, Michael J. Reeder
Formal analysis: Juliane Schwendike, Gareth J. Berry, Michael J. Reeder
Investigation: Juliane Schwendike, Katherine Fodor
Methodology: Juliane Schwendike, Gareth J. Berry, Michael J. Reeder
Visualization: Juliane Schwendike, Gareth J. Berry
Writing – review & editing: Juliane Schwendike, Gareth J. Berry, Katherine Fodor, Michael J. Reeder

Abstract This study investigates: (i) how the *local* meridional (Hadley) and zonal (Walker) circulations change in each phase of the Madden-Julian Oscillation (MJO); and (ii) the effect of enhanced and suppressed MJO-related convection on the poleward extent of the local Hadley circulations and, thus, the strengths and positions of the subtropical jets. We examine these effects in ERA-Interim reanalysis by decomposing the vertical mass flux into zonal and meridional components. We show for the first time, that as the envelope of enhanced convection moves eastwards from Africa to the Central Pacific the *local* Hadley circulation is enhanced. The *regional* Walker circulation in the Pacific is strengthened when the envelope of active MJO convection is located over the Maritime Continent and weakened when the region of suppressed convection is located there. In regions of anomalous upper-level divergence the subtropical jet is enhanced. The core of the subtropical jet over Asia shifts eastwards with the progression of the MJO and shifts farther poleward in regions of anomalous upper-level divergence linked with enhanced convection. The region of either enhanced or suppressed convection over the Maritime Continent strengthens or weakens the local Hadley circulation, producing disturbances in the subtropical jet. These disturbances then force midlatitude Rossby waves that propagate across the Pacific Ocean in both hemispheres.

1. Introduction

The definitions of the Hadley and Walker circulations are often based on zonal and meridional averages respectively (e.g., Barry & Carleton, 2001; Hartmann, 1994; L'Heureux et al., 2013; Julian & Chervin, 1978; Power & Smith, 2007; Tokinaga et al., 2012; Trenberth & Stepaniak, 2003; Vecchi et al., 2006). In reality though, these circulations are far from uniform in the zonal and meridional directions, and show considerable spatial variability, leading to the concept of *local* Hadley and Walker circulations (e.g., Schwendike et al., 2014, 2015). One of the most important sources of variability in the Tropics is the Madden-Julian Oscillation (MJO), which consists of a dipole of enhanced and suppressed convection that moves eastward from the tropical Indian Ocean to the Western Pacific with a period of 30–60 days (e.g., Madden & Julian, 1972, 1994; Zhang, 2005, 2013). Given the extensive overlap between the MJO and the Hadley and Walker circulations, it is expected that the MJO leads to significant variations in the strength and position of these circulations *locally*, yet there is no quantitative evidence of this in the literature. The purpose of this study, therefore, is to quantify the relationship between the *local* Hadley and Walker circulations and the MJO.

In addition to its link with the tropical circulation, MJO convection is known to impact the strength and position of the subtropical jet (e.g., Matthews & Kiladis, 1999; Moore et al., 2010), as well as to generate Rossby wave trains that propagate into the midlatitudes (e.g., Kiladis & Weickmann, 1992; Knutson & Weickmann, 1987; Sardeshmukh & Hoskins, 1988; Matthews et al., 2004; Hendon & Salby, 1994; L'Heureux & Higgins, 2008; Higgins & Mo, 1997; Lukens et al., 2017). The Rossby wave trains, generated by convection due to the MJO, have numerous impacts, for example, on the North Atlantic Oscillation (NAO) (e.g., Cassou, 2008; Lin et al., 2009), Pacific/North American teleconnections (e.g., Mori & Watanabe, 2008), the triggering of convection over the South Pacific Convergence Zone (SPCZ) (Matthews et al., 1996), and blocking in the Southern Hemisphere (e.g., Renwick & Revell, 1999).

Recent idealized modeling studies have investigated the link between MJO convection and the response in the midlatitudes. Shao et al. (2019), for instance, have shown that heating in the tropics related to the MJO is

the precursor for a midlatitude wave train in the Pacific with an anticyclonic anomaly over the northeastern Pacific and a positive NAO pattern in the Atlantic. The idealized general circulation model experiments of Zheng and Chang (2019) found that for a strong extratropical response, the MJO has to propagate through Phases 1–3 and 5–7, and that the response in the midlatidues depends on the propagation speed, initiation and decay of the MJO. Hall et al. (2020) have shown that the response to heating in the Indian Ocean is an anticyclone over the Pacific and low-pressure system over northwestern North America. They found the opposite pattern occurs when the heating is located in the Western Pacific.

These studies have provided important insights into the impact of the MJO in the midlatitudes, but overwhelmingly, they have concentrated on the Northern Hemisphere boreal winter. Here we extend that work by assessing MJO-induced changes to the subtropical jets, and the resulting midlatitude Rossby wave response, in both hemispheres and for both boreal and austral winter.

Overall, we seek to answer the following questions: i) How do the *local* Hadley and Walker circulations change in each phase of the MJO? ii) How does the MJO affect the poleward extent of the *local* Hadley circulations, and thus the subtropical jets and midlatitude Rossby wave response, both globally and seasonally? We investigate these questions by objectively decomposing the three-dimensional atmosphere into a pair of orthogonal overturning circulations, that is, *local* Hadley and *local* Walker circulations (Schwendike et al., 2014). The sum of the individual circulations equals the original, thereby allowing us to examine regional overturning circulations in an unambiguous way. The method and data used will be described in Section 2. The climatology of precipitation and the local Hadley and Walker circulations in different MJO phases will be shown in Section 3. Section 4 will investigate the influence of the location of the MJO convection on the subtropical jet using the flow decomposition framework. Section 5 will link the MJO and midlatitude Rossby waves. A summary and the conclusions will be given in Section 6.

2. Data and Method

Schwendike et al. (2014) have adapted the ψ-vector method, originally developed by Keyser et al. (1989), to decompose the tropical atmosphere into a pair of orthogonal overturning circulations, satisfying continuity independently in a Cartesian framework in spherical pressure coordinates. This pair of overturning circulations are the local Hadley and Walker circulations, respectively. The method is outlined below and full details can be found in Schwendike et al. (2014).

The meridional overturning circulation at a point or in a plane in the tropics is referred to as the local Hadley circulation, and the zonal overturning circulation at a point or in a plane in the tropics is referred to as the local Walker circulation. Outside of the tropics it is best to think of these circulations mainly as meridionally and zonally overturning circulations.

The vector stream function ψ is defined as

$$\nabla_p \cdot \psi = -\nabla_p^2 \mu = \omega, \tag{1}$$

where ∇_p is the horizontal gradient operator in isobaric coordinates, μ is a potential function, and ω is the vertical motion.

The vertical motion, ω, can be partitioned uniquely into the zonal and meridional planes according to:

$$\omega_\lambda cos\phi = \frac{1}{a}\frac{\partial \psi_\lambda}{\partial \lambda} = \frac{1}{a^2 cos\phi}\frac{\partial^2 \mu}{\partial \lambda^2}, \tag{2}$$

$$\omega_\phi cos\phi = \frac{1}{a}\frac{\partial}{\partial \phi}(\psi_\phi cos\phi) = \frac{1}{a^2}\frac{\partial}{\partial \phi}\left(cos\phi \frac{\partial \mu}{\partial \phi}\right), \tag{3}$$

where ω_λ and ω_ϕ are the vertical motion associated with flow in the zonal and meridional planes, ψ_λ and ψ_ϕ are the stream functions in the zonal and meridional directions, and a is the radius of the Earth. The

subscripts λ and ϕ indicate the zonal and meridional directions respectively. Thus, the upward mass fluxes associated with the zonal and meridional parts of the circulation are

$$m_\lambda = -\omega_\lambda cos\phi \,/\, g \qquad \text{and} \qquad m_\phi = -\omega_\phi cos\phi \,/\, g, \tag{4}$$

respectively, where g is the gravitational acceleration.

The adapted version of the ψ-vector method is applied to the European Centre for Medium range Weather Forecasts (ECMWF) ERA-Interim (ERAI) reanalysis data (Dee et al., 2011; Simmons et al., 2011) with a horizontal resolution of 0.75 degrees for the period 1979 to 2009. Additionally, the Tropical Rainfall Measuring Mission (TRMM) Multi-satellite Precipitation Analysis (TMPA-RT) 3-hourly data (product 3B42) between 1989 and 2009 with a horizontal resolution of 0.25° is used to examine precipitation anomalies in different phases of the MJO (Huffman et al., 2010). To divide the precipitation and mass flux data into the eight phases of the MJO the real-time multivariate MJO index, RMM, is used (Wheeler & Hendon, 2004). MJO events are selected when the amplitude of the RMM empirical orthogonal functions is one or greater.

We have carried out the same analysis for neutral ENSO phases only by separating the data based on the Southern Oscillation Index (SOI) from the Australian Bureau of Meteorology and chose a threshold of +5 for for La Niña events and −5 for El Niño events. We found that the results remain unchanged. The main difference was that the amplitudes of the fields shown below are higher for neutral ENSO days than when including all days due to the lower number of days in each composite.

3. Climatology of Hadley and Walker Circulations According to MJO Phase

The rainfall anomalies in different phases of the MJO based on 3-hourly TRMM data are calculated in this section and compared to the response of the local Hadley and local Walker circulations in the respective MJO phase.

3.1. Rainfall Anomalies

The eastward propagation of the envelope of enhanced MJO convection, that is, enhanced precipitation, from Africa to the Pacific has been well documented (e.g., Wheeler & Hendon, 2004). To motivate the present study, to remind us of the distribution of regions of enhanced and suppressed convection during different MJO phases, and most importantly to show the link between rainfall and the upward mass flux, we have plotted the TRMM precipitation anomalies in Figures 1 and 2.

The rainfall anomalies between 1989 and 2014 in December, January, February (DJF) are shown for different MJO phases in Figure 1, with every second phase shown for brevity. In Phase 2 of the MJO, the precipitation over the Indian Ocean is increased (Figure 1a) and the precipitation over the Maritime Continent and the Western Pacific is reduced. A significant precipitation increase also occurs over parts of China and the adjacent ocean. In Phase 4 (Figure 1b), the convection and associated precipitation are located over the Maritime Continent with notable regions of increased precipitation east of the Indian subcontinent, parts of Southeast Asia, along the inter-tropical convergence zone (ITCZ) and the SPCZ. Weaker increases in precipitation also occur along the storm tracks in the Northern Hemisphere. In Phase 6 (Figure 1c), precipitation is increased east of the Maritime Continent and in the Western Pacific as well as over northern Australia and the SPCZ. The positive precipitation anomaly continues to move eastward until it reaches the Central Pacific Ocean and enhances the SPCZ in Phase 8 (Figure 1d). In this phase precipitation is reduced over the Maritime Continent.

In June, July, and August (JJA), the eastward movement of enhanced convection is less pronounced, although the changes for the Maritime Continent are distinct (Figure 2). In Phase 2 (Figure 2a), there is suppressed precipitation over large parts of the Maritime Continent and enhanced precipitation occurs over and south of India as well as large parts of Indonesia. In Phase 4 (Figure 2b), the band of increased precipitation extends farther into the Western Pacific. Precipitation increases also along a band ranging from

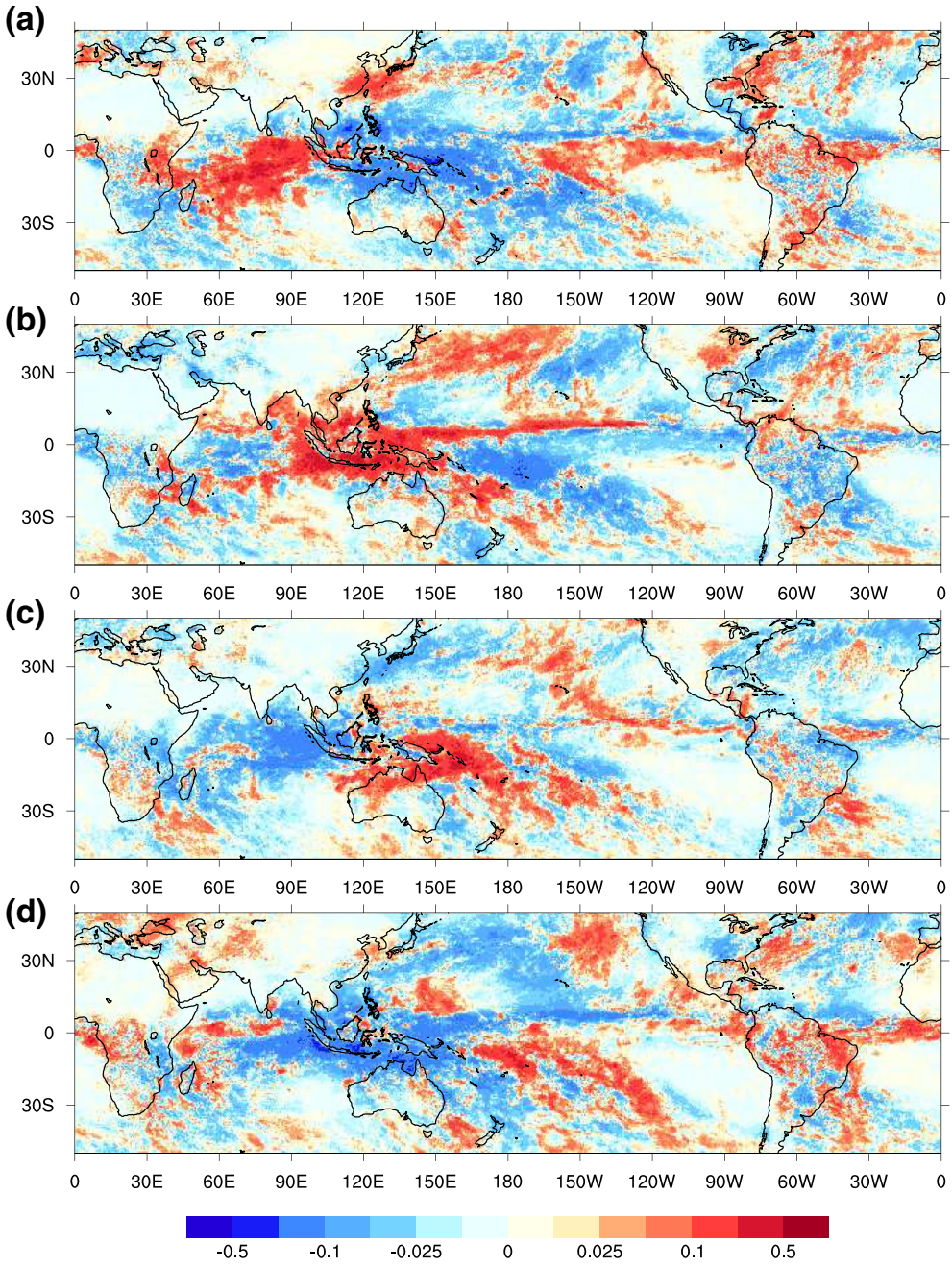

Figure 1. TRMM precipitation anomalies (mm h^{-1}) relative to the mean between 1989 and 2014 in MJO phases (a) 2, (b) 4, (c) 6, and (d) 8 in DJF. TRMM, Tropical Rainfall Measuring Mission; MJO, Madden-Julian Oscillation; DJF, December, January, February.

India to the ITCZ in the Western Pacific. In Phase 6 (Figure 2c), the anomaly in precipitation is largest in the Western Pacific and north of the Equator, along the ITCZ. Precipitation also increases along the storm tracks in the Southern Hemisphere. In Phase 6, precipitation is reduced over the Central and Eastern Indian Ocean and large parts of Indonesia and Malaysia. Phase 8 (Figure 2d) is characterized by mainly reduced precipitation. Precipitation is enhanced in the Eastern Pacific and over South America.

In most MJO Phases in DJF and JJA, a positive precipitation anomaly occurs on either side of the equator in the Eastern Pacific, potentially indicating a double ITCZ as pointed out in Berry and Reeder (2014). These

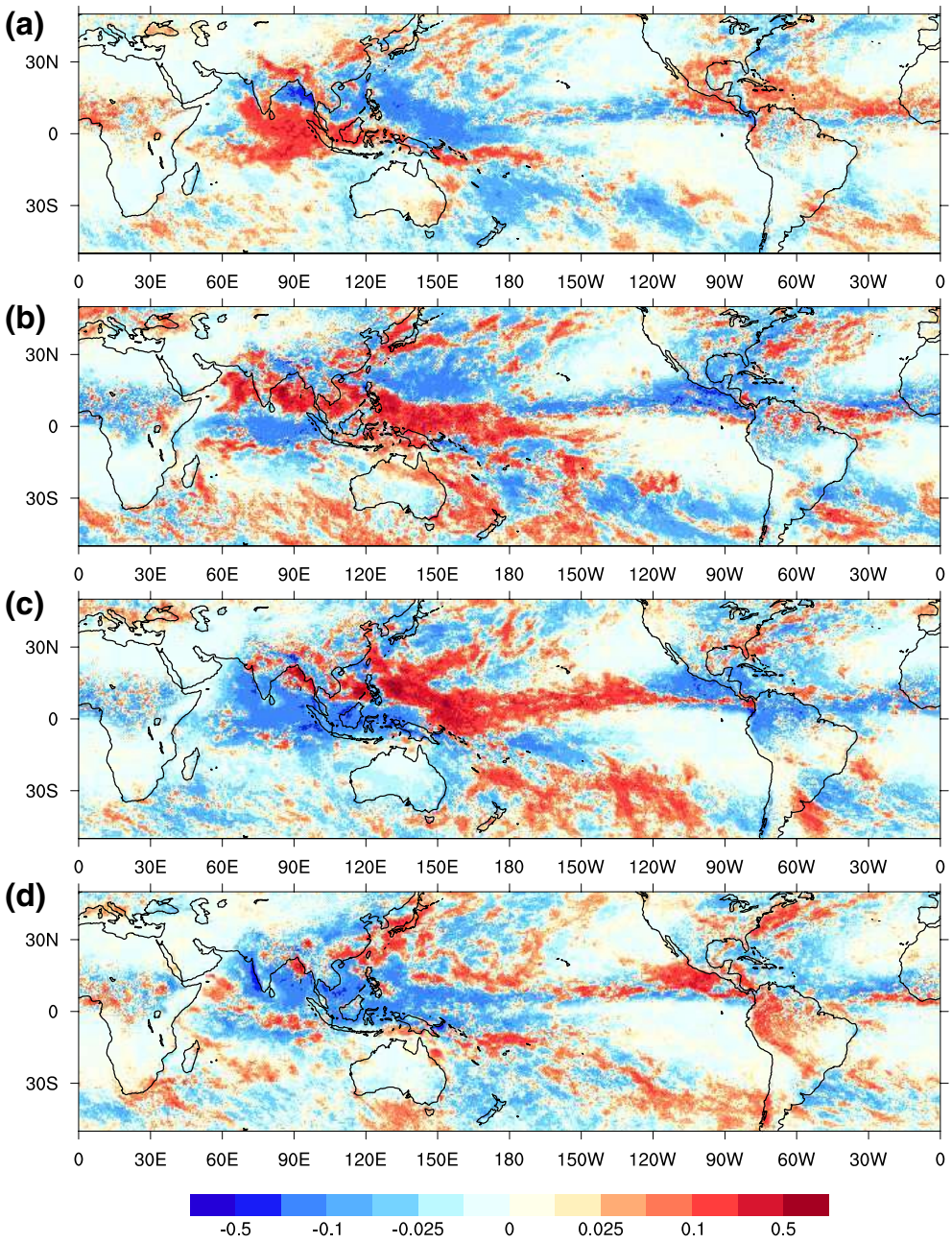

Figure 2. The same as Figure 1, but for JJA. JJA, June, July and August.

positive precipitation anomalies disappear or weaken when the active (e.g., Phase 2) or suppressed (e.g., Phase 6) MJO convection is located in the Indian Ocean.

3.2. Mass Flux Anomalies

The eastward movement of an envelope of convection and the associated precipitation from Africa to the central Pacific Ocean (Figures 1 and 2) is also reflected in the anomalies of the 500-hPa mass flux. The meridional and zonal mass flux anomalies at 500 hPa during DJF are shown in Figures 3 and 4, respectively. These mass flux anomalies represent the anomalies in the local Hadley (meridional) and Walker (zonal) circulations associated with the MJO.

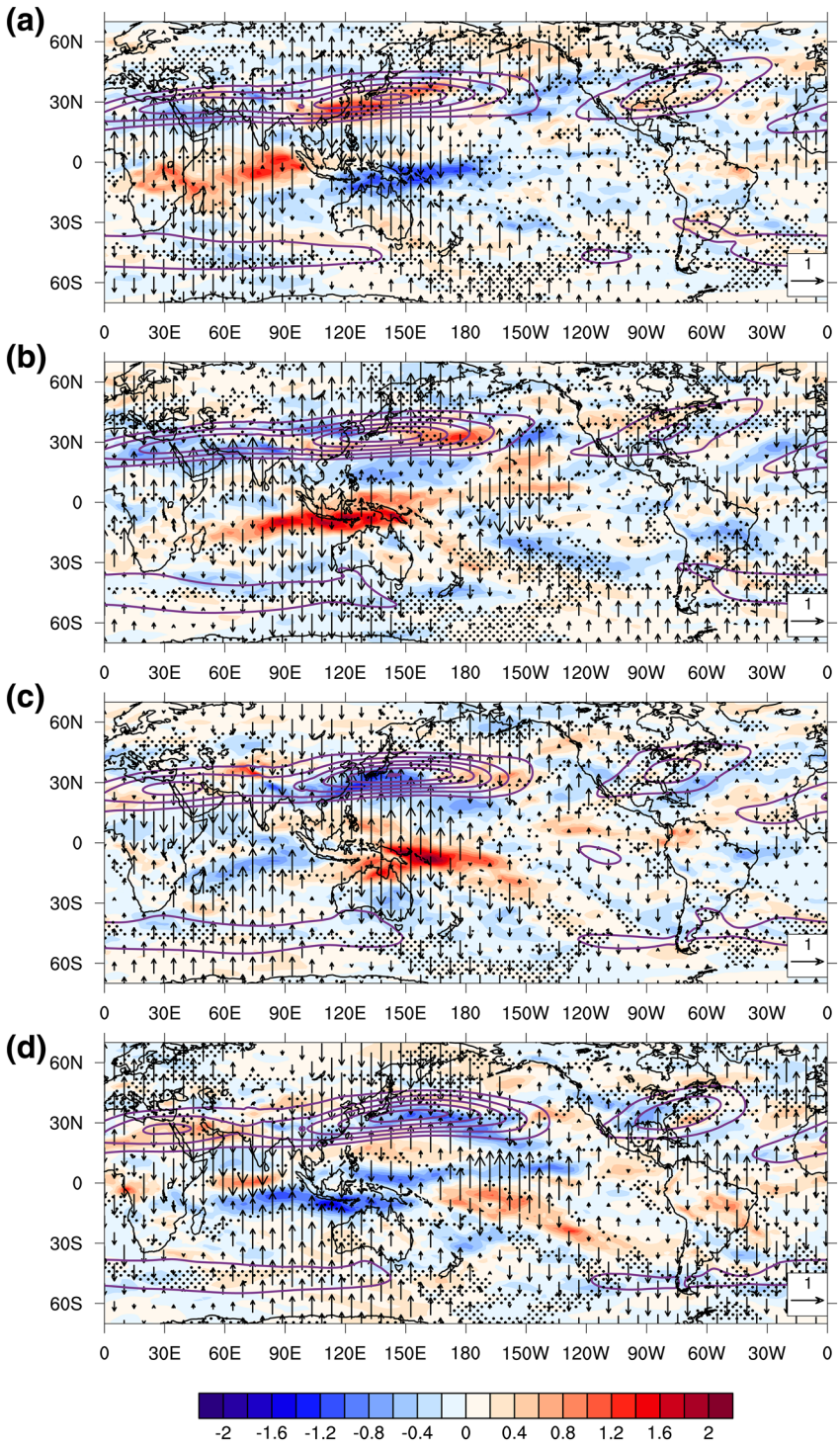

Figure 3. Meridional mass flux anomalies at 500 hPa (shaded, kg m^{-2} s^{-1}) and the anomalous divergent meridional wind component at 200 hPa (arrows, m s^{-1}) in (a)–(d) MJO phases 2, 4, 6, and 8 in DJF between 1979 and 2009. The purple contours show the total windspeed greater than 30 m s^{-1}, with the outermost contour representing 30 m s^{-1}, in intervals of 10 m s^{-1} at 200 hPa. The black stipples indicate regions where the meridional mass flux anomalies are not statistically different from the mean between 1979 and 2009 at the 95% confidence level. MJO, Madden-Julian Oscillation.

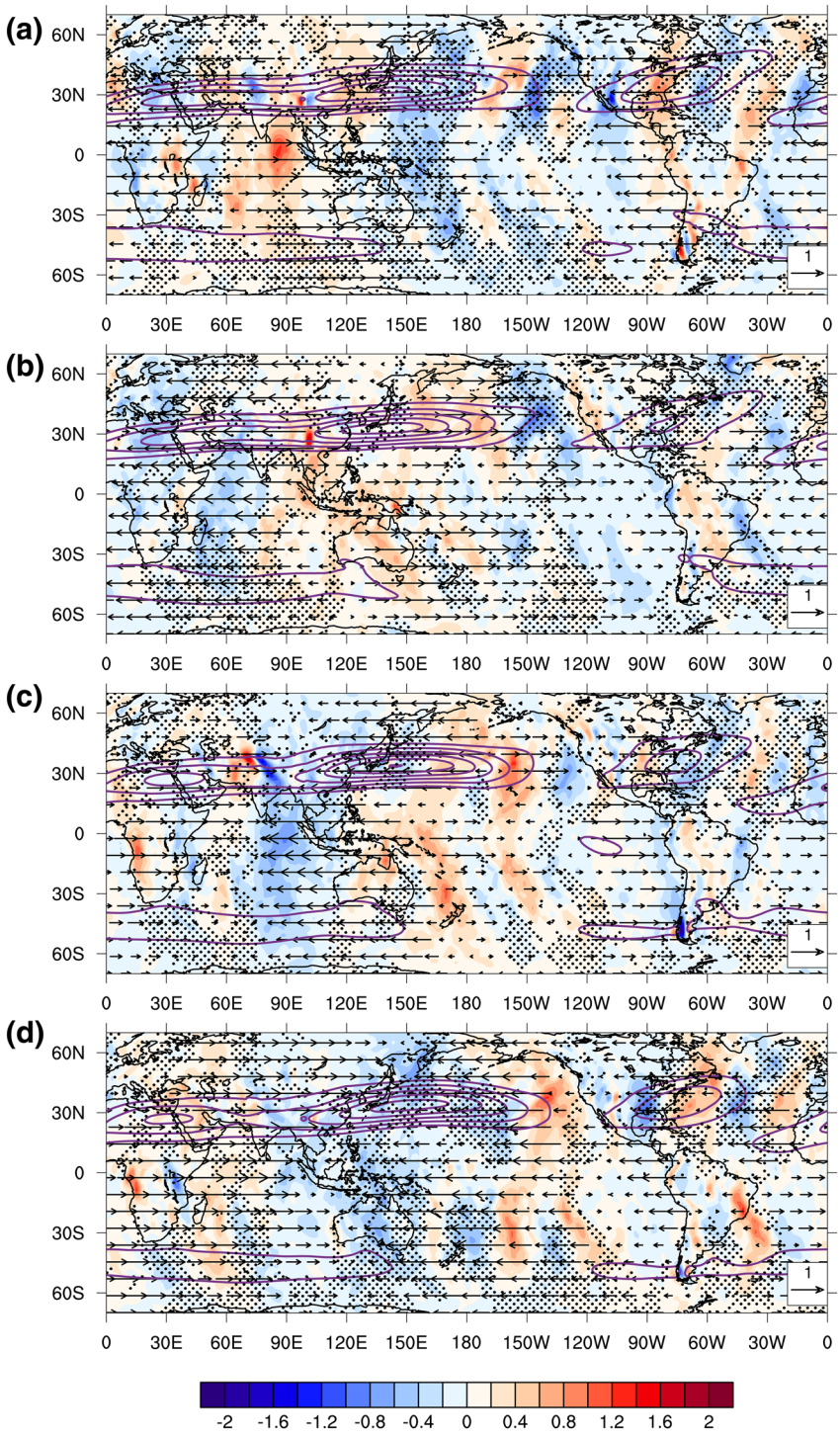

Figure 4. Same as Figure 3, but for the zonal mass flux anomalies and the anomalous zonal component of the divergent wind.

The statistical significance of the mass flux anomalies has been determined through bootstrapping (Hesterberg et al., 2003) with 1,000 random anomaly patterns of the meridional mass flux for each time of the ERAI data. The stipples indicate regions where the meridional mass flux anomalies are not statistically significant

from the mean meridional mass flux between 1979 and 2009 at the 95% confidence level. The statistical significance for the anomalies in the remainder of the paper has been calculated in the same manner.

In Phase 2 (Figure 3a) the local Hadley circulation is enhanced over the Indian Ocean (between 1 and 2 $kg\,m^{-2}s^{-1}$), and over the Maritime Continent in Phase 4 (Figure 3b). In Phase 6 (Figure 3c), the local Hadley circulation is stronger (1–2 $kg\,m^{-2}s^{-1}$) than the mean local Hadley circulation over the eastern parts of the Maritime Continent and the Western Pacific. The upward mass flux is increased by about the same amount along the SPCZ and the local Hadley circulation is weakened by about 1–1.5 $kg\,m^{-2}s^{-1}$ over the Indian Ocean. In Phase 8 (Figure 3d), the mass flux is weaker (by about 1–2 $kg\,m^{-2}s^{-1}$) over large parts of the Maritime Continent, whereas over the SPCZ it is enhanced (by about 0.4–1.2 $kg\,m^{-2}s^{-1}$). These changes in meridional mass flux are consistent with the changes in precipitation (Figure 1).

The divergent part of the wind in the meridional direction at 200 hPa shows that divergence occurs in regions of enhanced upward mass flux consistent with the divergent outflow from regions of deep convection. The region of upper-level divergence moves eastwards with the enhanced precipitation. In regions of suppressed precipitation the divergent part of the wind in the meridional direction at 200 hPa converges and reduced upward mass flux occurs.

The local Walker circulation shows a similar amplitude of changes to the MJO phase as the local Hadley circulation (Figure 3), although the local Walker circulation climatologically is about a factor two weaker than the local Hadley circulation (Schwendike et al., 2014). The change in the local Walker circulation for each of the phases of the MJO (Figure 4) is similar to the corresponding changes in the local Hadley circulation and the eastward propagation of the envelope of enhanced convection is distinct.

Moreover, Figure 4 shows that quasi-stationary midlatitude waves occur downstream of the regions of either enhanced or suppressed upward mass flux over the Maritime Continent. The extratropical wave pattern occurs in all MJO phases across most longitudes. Not only does the MJO affect the strength of the local Hadley and Walker circulations, the regions of enhanced and suppressed MJO precipitation are co-located with the origin of a midlatitude wave train as we will show in Section 5. These midlatitude wave trains occur in both hemispheres where they appear to be quasi-stationary relative to the forcing (the MJO) as a propagating wave signal would have been averaged out.

Broadly speaking, a similar pattern of mass flux anomalies and distribution of the divergent part of the wind are also found in JJA, although the details of where the regions of enhanced and weakened mass flux are located are different (Figures 5 and 6). For instance, in Phase 2 the anomalous upward meridional mass flux is larger over the western Indian Ocean and Malaysia than in the mean (Figure 5a). Over large parts of Australia, the anomaly is positive, and over Thailand and the South China Sea the anomaly is strongly negative. In Phase 4 (Figure 5b), there is an almost continuous band of enhanced upward mass flux located near or north of the Equator ranging from Africa to the Americas. This band is located farther north over the Indian Ocean, India and parts of the Maritime Continent. A negative meridional mass flux anomaly occurs north of the region of enhanced mass flux in the Pacific Ocean. In Phase 6 (Figure 5c), mass flux decreases over large parts of the Maritime Continent, the Indian Ocean and Australia. The mass flux is enhanced (by about 1.2 to over 2 $kg\,m^{-2}s^{-1}$) over Thailand, Southern China, the South China Sea and the Philippines. In Phase 8 (Figure 5d), the northern part of the Maritime Continent is characterized by negative mass flux anomalies (about 1.2 to over 2 $kg\,m^{-2}s^{-1}$), but the northern part of Australia and the eastern Pacific show weakly positive meridional mass flux anomalies (about 0.4–1 $kg\,m^{-2}s^{-1}$).

When comparing the anomalies of the zonal mass flux for each MJO phase between DJF (Figure 4) and JJA (Figure 6), it is apparent that the midlatitude wave trains are more pronounced in the winter hemisphere than in the summer hemisphere. The distribution of mass flux anomalies is relatively similar between JJA and DJF; however, the divergent part of the wind in the zonal direction shows differences.

This analysis shows that the local Hadley circulation strengthens (weakens) by 50% of its climatological mean when it coincides with the envelope of enhanced (suppressed) MJO convection. The absolute changes to the local Walker circulation are similar to those of the local Hadley circulation, but due to being climatologically a factor of two weaker than the local Hadley circulation, the local Walker circulation doubles in

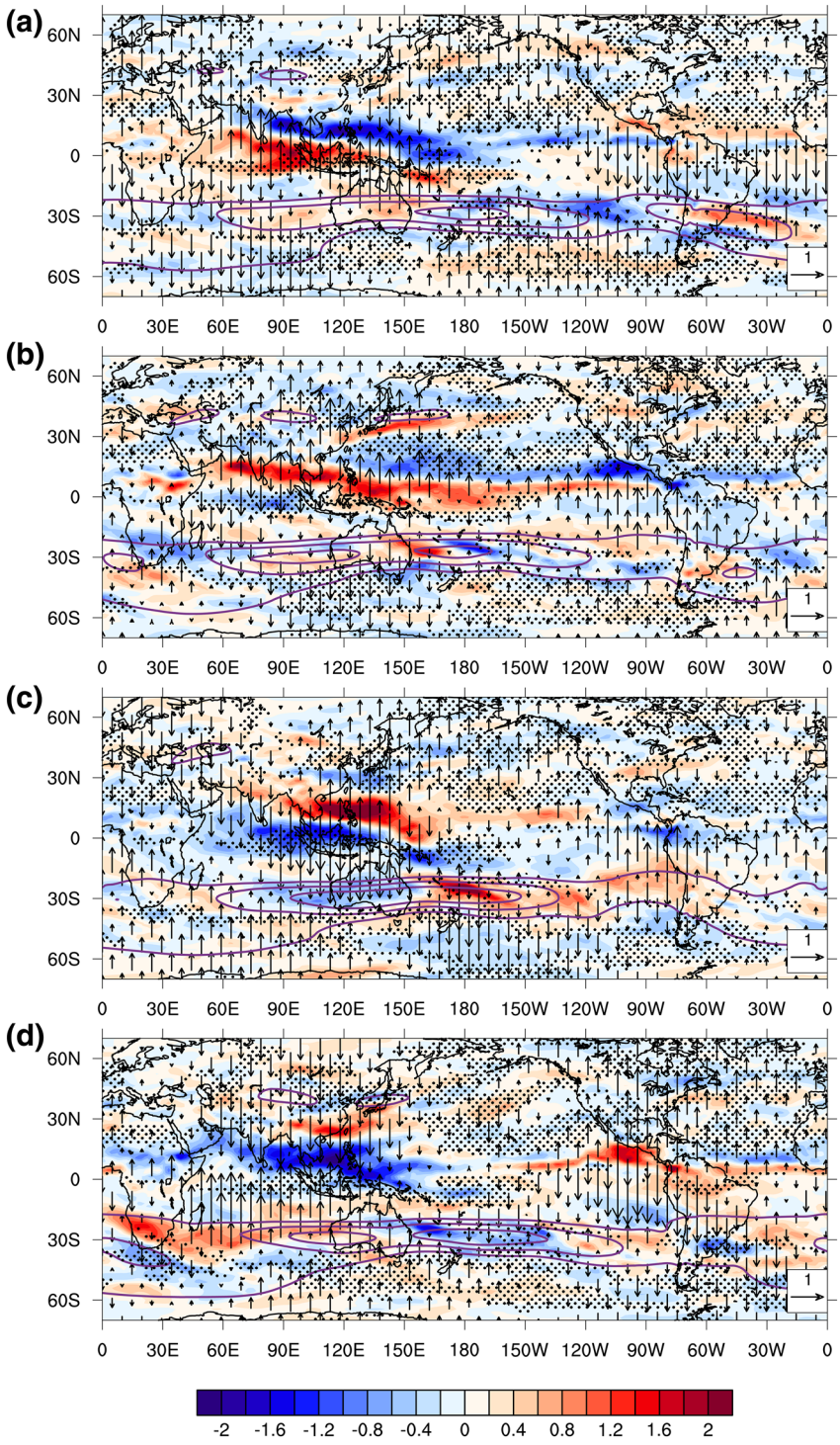

Figure 5. Same as Figure 3, but for JJA. JJA, June, July and August.

strength when the MJO convection is located over the Maritime Continent and is almost completely suppressed when the weakened MJO convection is located over the Maritime Continent.

The large magnitude of these changes to the tropical circulation have consequences that extend well into the midlatitudes. In the following sections, we discuss the changes to the subtropical jet and the midlatitude

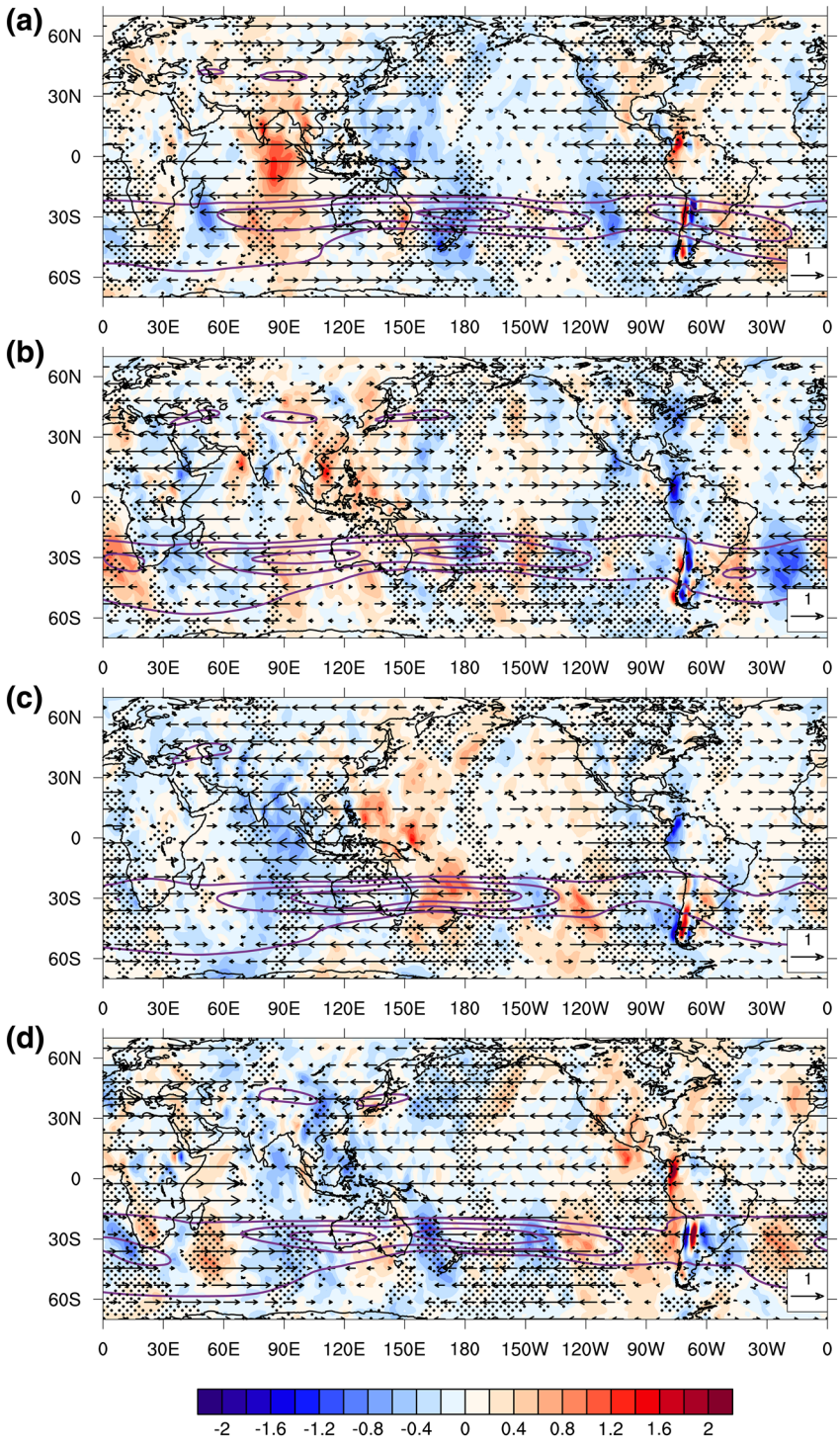

Figure 6. Same as Figure 4, but for JJA. JJA, June, July and August.

Rossby wave response, with an emphasis on the differences from Northern Hemisphere winter that has been the focus of past studies.

4. MJO and the Subtropical Jet

To address how the propagation of the envelope of enhanced and suppressed convection affects the poleward extent of the local Hadley circulations and the subtropical jets we will analyze how the position and the strength of the subtropical jet changes during different phases of the MJO, and we will quantify changes in the jet over selected regions.

4.1. Windspeed Anomalies

The subtropical jet is illustrated with the 200-hPa wind speeds larger than 30 m s^{-1} in Figures 3–6. In DJF, the strongest jet extends from North Africa to Asia with the maximum located between 25°N and 45°N over Japan and the Western Pacific. A weaker but pronounced jet exists on the southern and eastern flank of North America with the maximum located over the east coast (Figure 3). The jet in the Southern Hemisphere is weaker, as expected, and extends from South America to Australia. The jets are located at the poleward edges of the descending branch of the local Hadley circulation (see Figure 1 in Schwendike et al. (2014)).

In JJA in the Northern Hemisphere, wind speeds larger than 30 m s^{-1} only occur over Asia (e.g., Figure 5). In the Southern Hemisphere, a band of wind speeds exceeding 30 m s^{-1} is located roughly between 25°S and 50°S. Maxima in wind speed occur east and west of Australia and east of South America.

To illustrate the changes in the subtropical jets in different MJO phases, the differences between the mean windspeed between 1979 and 2009 and the mean windspeed in each MJO phase in DJF and JJA are shown in Figures 7 and 8. In DJF in Phase 2 of the MJO the convection occurs over the Indian Ocean in a region of upper-level divergence (Figure 7a). North of the region of enhanced convection, at around 30°N, the jet speed is increased by about 8–10 m s^{-1}. East of this region, where the jet is climatologically strongest, the jet is weakened by about 5–10 m s^{-1}, an area characterized by convergence over the Maritime Continent. The jet along the storm track over North America and the Atlantic is strengthened by about 3–6 m s^{-1}.

In Phase 4 (Figure 7b), the wind speed east of the mean maximum of the jet, which is located roughly over Japan, is reduced, and increased west of the region of the maximum. The increase in wind speed to the west of the maximum is consistent with the strong divergent outflow of the convection located over the western part of the Maritime Continent. The region east of the mean jet maximum is characterized by upper tropospheric convergence.

As the envelope of MJO convection moves farther toward the east, the region of increased upper-level wind speed also moves eastward. In Phase 6 (Figure 7c), the wind speed is increased in the region of the mean maximum of the jet, and weakened west of it. In Phase 8 (Figure 7d), the jet is strengthened east of the climatological maximum and weakened west of this region.

In JJA, the same patterns can be seen. In Phase 2 (Figure 8a), the speed of the subtropical jet is increased over South Africa and west of Australia in a region characterized by upper-level divergence. Over southern Australia and east of Australia, the wind speed decreases in a region of upper-level convergence. In Phase 4 (Figure 8b), the wind speed increases farther over the Southern Ocean and extends farther to the east. Similarly, the wind speed decreases over southeastern Australia and at around 30°S east of Australia. In Phase 6 (Figure 8c), when the convection is located over the eastern side of the Maritime Continent, the jet is enhanced and has a maximum over southern Australia. Over South Africa the wind decreases. As the convection moves farther east into the Western Pacific Ocean, the region of increased wind speed also moves eastwards. In Phase 8 (Figure 8d), the jet maximum is located in the South Pacific Ocean. The jet is weakened south of South Africa, the Indian Ocean and parts of Australia.

Comparing the intensity of the winter hemispheric jets between Phases 4, 6 and Phases 8, 2 (Figures 7 and 8) shows that the jet over Australia is stronger between about 90°E and 150°E in Phase 6 than in Phases 8, 2, when the enhanced convection is located over the Maritime Continent. When the convection is located over the Western Pacific, the jet has a local maximum over the Western Pacific (Figure 8d). A similar behavior occurs for the subtropical jet located over Africa, Asia and the northern Pacific and the jet over North America and the North Atlantic.

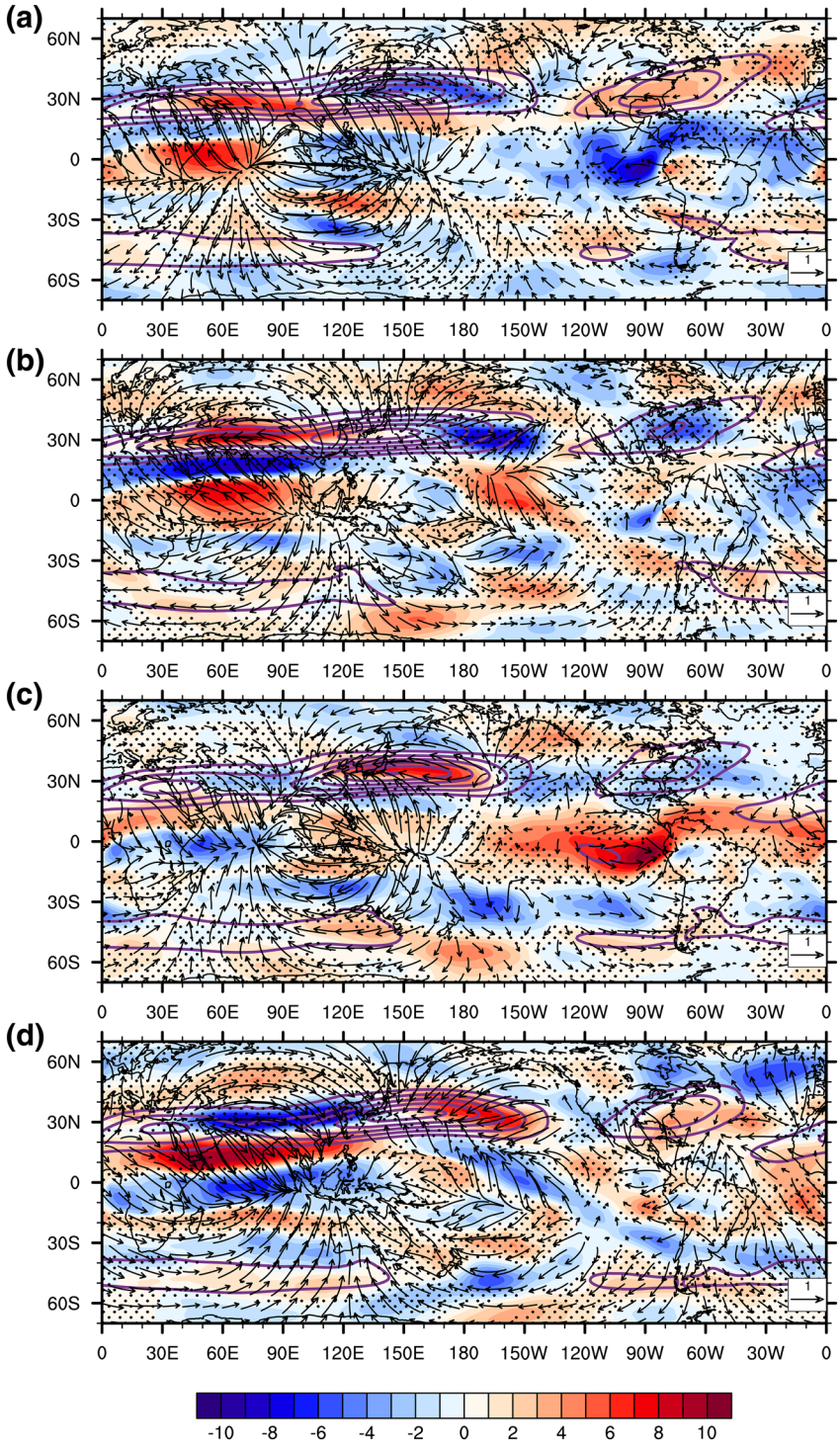

Figure 7. Wind speed anomalies (shaded, m s^{-1}) and the divergent wind anomalies at 200 hPa (arrows, m s^{-1}) in (a)–(d) MJO phases 2, 4, 6, and 8 in DJF between 1979 and 2009. The contours show the total windspeed greater than 30 m s^{-1} in intervals of 10 m s^{-1} at 200 hPa. The black stipples indicate regions where the wind speed anomalies are not statistically different from the mean between 1979 and 2009 at the 95% confidence level. MJO, Madden-Julian Oscillation; DJF, December, January, February.

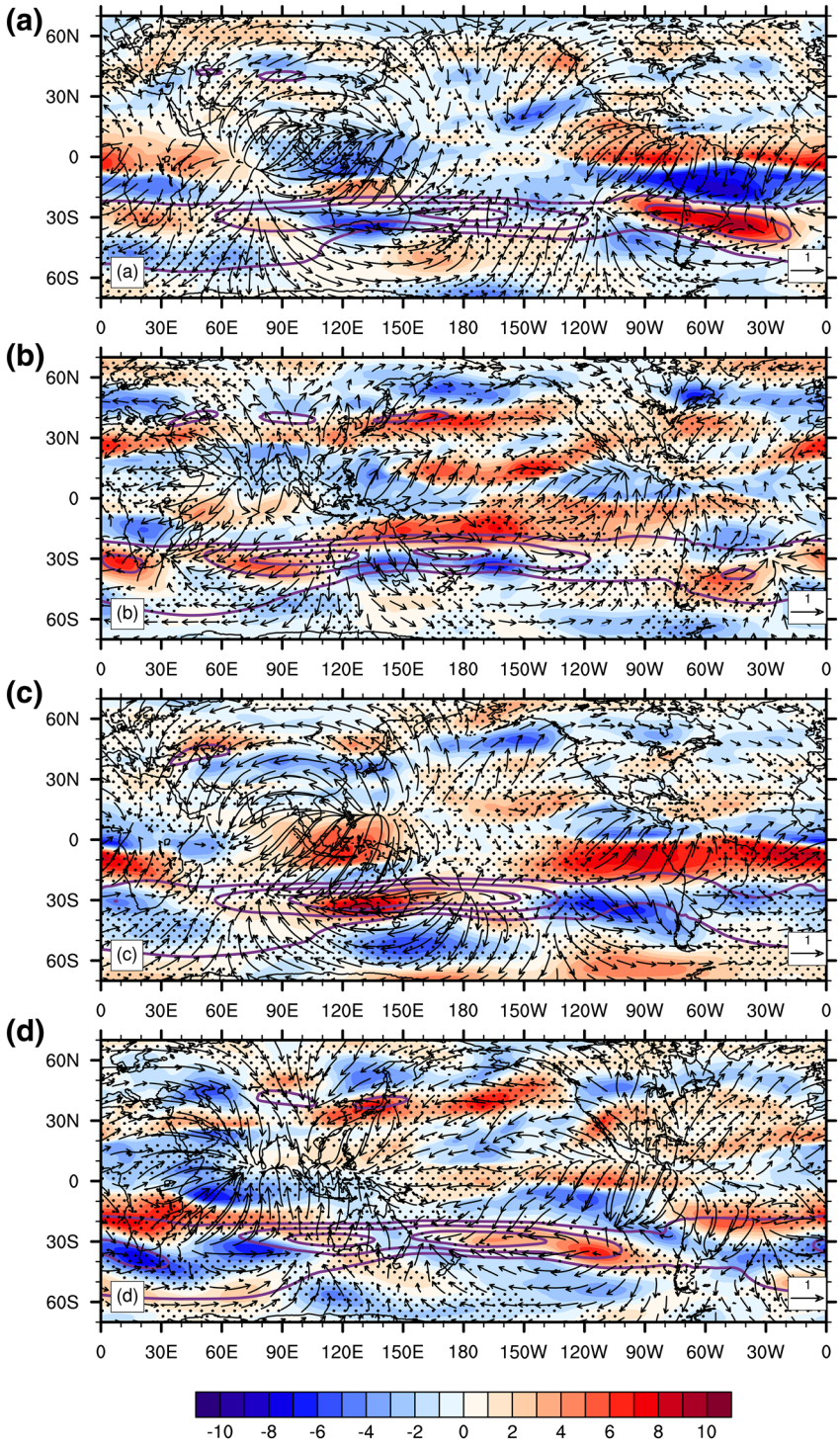

Figure 8. Same as Figure 7, but JJA. JJA, June, July and August.

While we focus here more on the changes in the midlatitudes, it is worth pointing out that there are significant changes in upper-level wind speed in the tropics. These wind speed anomalies are similar to those discussed in Zurita-Gotor (2019), who found that the large-scale eddy momentum transport in the tropics is associated with the correlation between the divergent meridional velocity and the non-divergent zonal

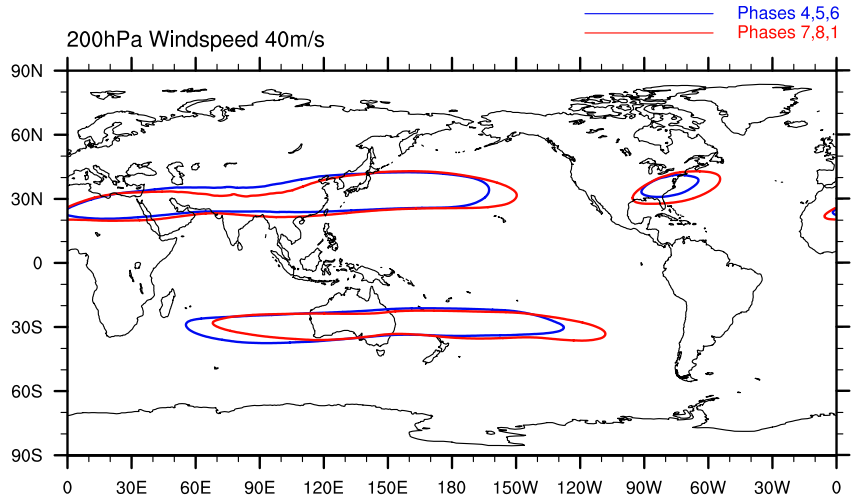

Figure 9. The 40-m s^{-1} contour is shown in blue averaged over MJO phases 4, 5, 6 and in red averaged over MJO phases 7, 8, 1 for the winter hemispheres, that is, DJF in the Northern Hemisphere and JJA in the Southern Hemisphere. MJO, Madden-Julian Oscillation; DJF, December, January, February; JJA, June, July and August.

velocity. They also pointed out that the Hadley circulation plays the dominant role in the tropical momentum transport.

In summary, the strengthening (weakening) of the jet due to upper-level divergence (convergence) associated with the MJO is strongest in the winter hemisphere. The magnitude of these changes remains similar between Northern and Southern Hemisphere winter.

4.2. Changes in the Jet Core Location

The analysis of the wind speed anomalies shows a relationship between the divergent outflow of the convection related to the MJO and the strengthening or weakening of the subtropical jet predominantly in the winter hemisphere when the jet is strongest. Figures 7 and 8 already indicated that there is a shift in the location of the jet core. For instance, the subtropical jet over India is displaced further northwards when the active phase of MJO convection is located over the Indian Ocean. At the same time, the subtropical jet in the southern Indian Ocean is displaced further poleward. To emphasize this relationship, the position of the jet core in both winter hemispheres (i.e., DJF in the Northern Hemisphere and JJA in the Southern Hemisphere) is shown in Figure 9.

When the envelope of active MJO convection is located over India and the Maritime Continent, the jet over Asia is located about 3–5° farther northwards compared to when the envelope of convection is located in the Western Pacific (Figure 9). The jet maximum over Asia extends by about 10° farther to the East during phases 7, 8, 1 when the active convection is located over the Western and Central Pacific and over eastern Africa. The increase in wind speed and extension to the north is consistent with the strong divergent outflow of the region of enhanced convection.

An eastward shift by about 10° can also be observed for the Southern Hemisphere jet located over Australia during Phases 7, 8, 1 compared to the location of the jet maximum in Phases 4, 5, 6. The jet also extends farther poleward in the Southern Hemisphere when the region of enhanced convection is located over in the Indian Ocean in Phases 4, 5, 6 and slightly poleward when the convection is located in the Central Pacific, but only by about 1–3° (Figure 9).

Our analysis shows that in the winter hemisphere, the jet is shifted polewards in regions of enhanced MJO convection and upper-level divergence, whereas in regions of suppressed convection and upper-level convergence, the location of the jet does not change.

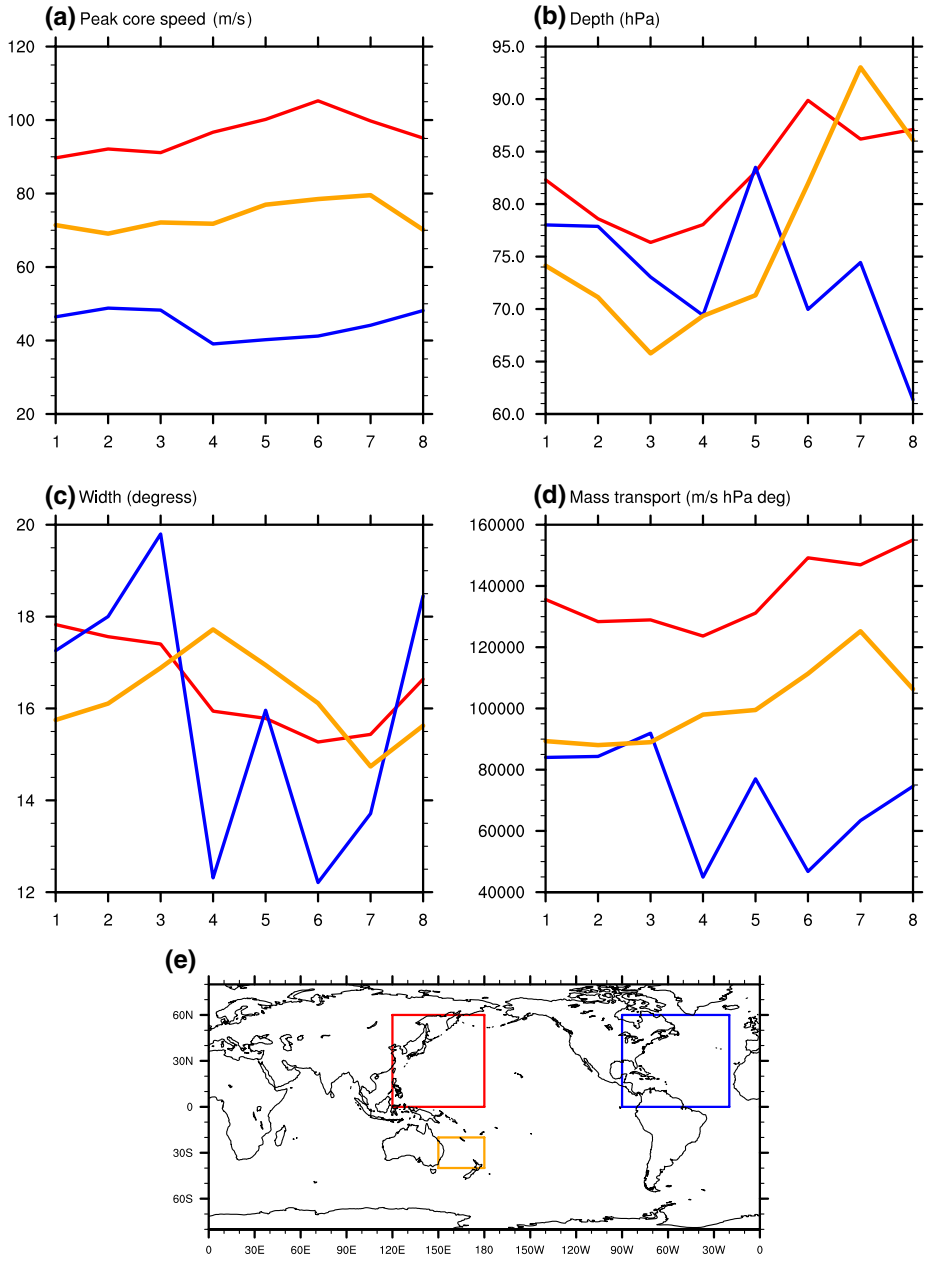

Figure 10. (a) The maximum jet core wind speed ($m\,s^{-1}$), (b) the depth of the jet (hPa), (c) the width of the jet (degrees), and (d) the mass transport ($m\,s^{-1}$ hPa degree^{-1}) for the boxes shown in (e). The red line shows the average over the red box over the Northwestern Pacific, the blue line shows the average over the blue box over the Northern Atlantic, and the orange line displays the average over the orange box located over eastern Australia and the Southwestern Pacific. The box averages are shown for the winter hemispheres, that is, DJF for the box over the Northwestern Pacific and the Northern Atlantic, and JJA for the box over the Southwestern Pacific. The MJO phase is given on the abscissa. MJO, Madden-Julian Oscillation; DJF, December, January, February; JJA, June, July and August.

4.3. Changes in Jet Core Characteristics Over Different Regions

In this section we consider the impact of the MJO on the jet in winter for three particular regions where this has not previously been studied: the Northwestern Pacific, the Southwestern Pacific and the North Atlantic.

To isolate the changes in the jet maxima with different MJO phases, in Figures 10 and 11 we show the jet core wind speed, the jet width and depth, as well as a measure of the mass transport, which is the product of

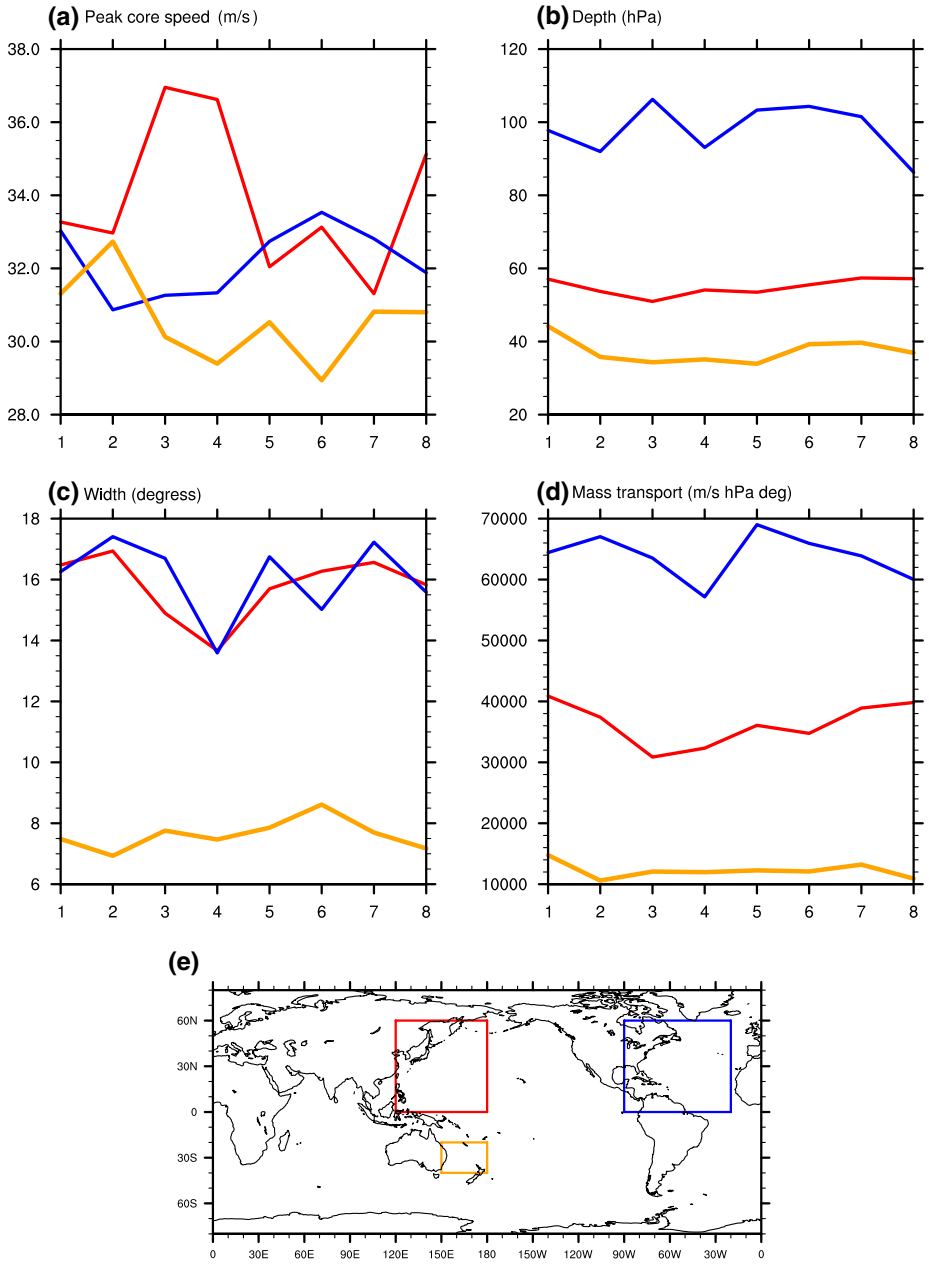

Figure 11. The same as in Figure 10 but for the summer hemispheres.

the three fields for three areas, that is, the Northwestern Pacific, the Northern Atlantic and the Southwestern Pacific (the three boxes shown in Figures 10e and 11e).

The jet location was determined by the zero-shear-vorticity line in regions where the wind speed was greater than 20 $m\,s^{-1}$, similar to the definition of the African Easterly jet axes in Berry et al. (2007). Then the line joining algorithm used in Berry et al. (2011) was applied to define the jet core. The jet widths are defined at each point along the jet by using the jet points either side to define a direction and scanning perpendicular to that to find where the wind speed drops to 2/3 of the core value. Likewise, the depth is computed by determining at what level the jet speed at each jet point drops to 2/3 of the core value.

In winter (Figure 10), the variability between MJO phases is high. The jet over the Northwestern Pacific reaches its maximum peak core speed in Phase 6 and its minimum in Phase 1. The peak core speed of the

Northwestern Pacific jet in DJF is larger than 100 m s^{-1}, which makes it the strongest jet of the three. The jet maximum is reached in Phase 7 in the Southwestern Pacific (JJA), and in Phases 1, 2, 3, and 8 over the Atlantic. As the jet core speed increases for the Northern and Southern Pacific jets, the depth of the jet (Figures 10b and 10e) and the mass transport (Figures10d and 10e) increase, but the jet width decreases (Figures 10c and 10e). The jet in the Northern Atlantic (DJF) shows a different behavior: the depth, width and mass transport do not vary coherently with MJO phase. This different behavior of the jet in the North Atlantic might be due to the fact that the anomalies at upper levels due to the MJO convection do not directly reach the North Atlantic. The changes in the subtropical jet in the Pacific are the direct response to tropical heating, but the changes to the jet in the Atlantic are likely due to the remote responses driven by wave propagation.

In summer (Figure 11) over the Northwestern Pacific (JJA), the jet core speed has its maximum with over 36 m s^{-1} in Phases 3 and 4. The depth of the jet (Figure 11b) remains relatively constant throughout all MJO phases. As the jet maximum increases, the width of the jet decreases (Figure 11c), and the mass transport decreases (Figure 11d). The changes in the jet structure over the Atlantic with MJO phase are different to the Northwestern Pacific. The jet core speed in DJF is largest in Phases 1, 5, 6, and 7 and weakest in Phase 2 (Figure 11a). The depth of the jet is nearly twice the depth of the jet located over the Northwestern Pacific, and changes only little from phase to phase. The evolution of the width of the jet is very similar to that in the Northwestern Pacific. In accordance to the larger depth of the jet in the North Atlantic is the larger mass transport in this region. The changes in Northern Hemisphere jet wind speed, jet depth and mass transport are distinct between MJO phases. The largest differences occur in the width of the jet. The jet is narrower in Phases 3–5 and wider in the other phases.

In summer over the Southwestern Pacific (DJF), the jet reaches its maximum wind speed in Phase 2 and the peak core speed is smallest in Phase 6. The jet is deeper when the core speed is high, and the jet is widest when the wind speed is lowest. Overall the depth of the jets and the mass transport change relatively little from phase to phase.

To summarize this section, we find that over the Northwestern and Southwestern Pacific, the jet core speed, depth and mass flux increase, while the jet width decreases when the active phase of convection is over the Maritime Continent. The jet in the Northern Atlantic also changes but the behavior is more erratic and does not vary coherently with MJO phase.

5. MJO and Midlatitude Rossby Waves

Many studies have shown a link between enhanced MJO convection and midlatitude Rossby waves, often by making use of the Rossby wave source and the wave-activity flux. Here, we use these well-established tools, but in contrast to previous studies, we calculate both fields for all MJO phases and for both the Northern and Southern Hemisphere during DJF and JJA. We use these calculations in conjunction with what we found in the previous sections to investigate the role of the divergent part of the wind in perturbing the jet.

5.1. Rossby Wave Source

To investigate the downstream impact of the changes in the midlatitude jets due to the enhanced and suppressed convection in the tropics, we calculated the Rossby wave source, S, as defined in Sardeshmukh and Hoskins (1988):

$$S = -\mathbf{v}_{div} \cdot \nabla_p \eta - \eta D = -\nabla_p \cdot (\mathbf{v}_{div} \eta), \tag{5}$$

where η is the absolute vorticity, D is the divergence of the wind, and $\mathbf{v}_{div}$ is the divergent part of the wind.

Additionally, we calculated the wave-activity flux based on Equation 38 in Takaya and Nakamura (2001). The wave-activity flux identifies stationary wave disturbances and indicates where the waves are emitted, refracted, and absorbed. The wave-activity flux is derived from quasi-geostrophic theory and therefore has limitations in the tropics. The two most important properties of the wave-activity flux are that: (i) the

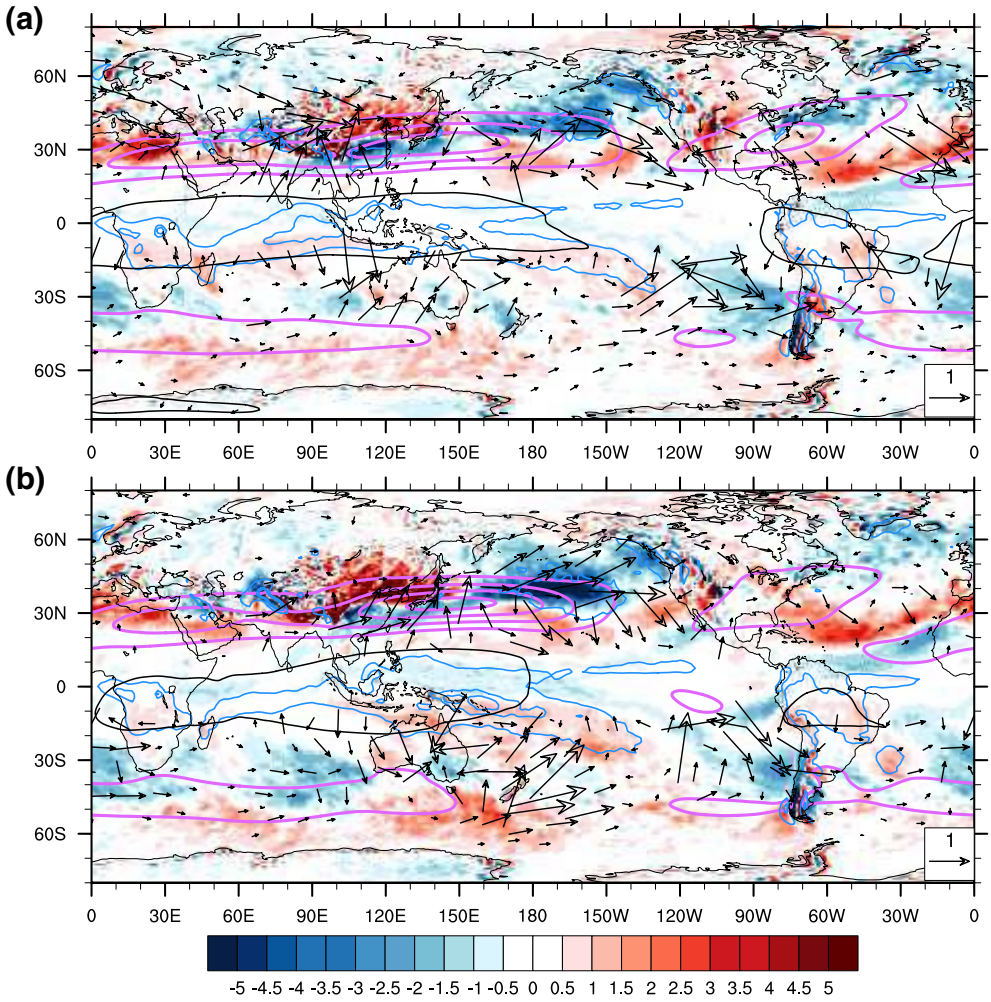

Figure 12. The Rossby wave source (shaded, 10^{-11} s^{-1}) and the wave-activity flux vector (arrows; midpoints of the arrows are centered on the grid points) at 200 hPa averaged over MJO phases (a) 2 and (b) 6 in DJF. The black contour displays the wave phase speed $C_p = 0$. The purple contours show the 200-hPa total windspeed greater than 30 $m\,s^{-1}$ in intervals of 15 $m\,s^{-1}$. The blue contour shows the meridional mass flux at 500 hPa greater than 0.002 $kg\,m^{-2}s^{-1}$ in intervals of 0.004 $kg\,m^{-2}s^{-1}$. MJO, Madden-Julian Oscillation; DJF, December, January, February.

convergence and divergence of the wave-activity flux vector can be related to changes in the amplitude of the wave; and (ii) the wave-activity flux shows the instantaneous wave packet propagation of stationary disturbances and the wave-activity flux vector is proportional to the group velocity.

The Rossby wave source and the wave-activity flux (not the anomalies) at 200 hPa in DJF and JJA are shown for Phases 2 (suppressed convection over the Maritime Continent) and 6 (enhanced convection over the Maritime Continent) in Figures 12 and 13. These figures show that disturbances in the jet, initiated from both enhanced upper-level outflow (enhanced convection) and upper-level convergence (suppressed convection), which can be interpreted as a strengthened or weakened local Hadley circulation, can lead to the formation of a quasi-stationary wave pattern along the jet in the Pacific Ocean. This result agrees with Sardeshmukh and Hoskins (1988), who found that the advection of absolute vorticity by the divergent flow in an equatorial region with easterly winds (which do not support Rossby waves) can lead to a Rossby wave source in the subtropical westerlies.

In DJF in Phase 2, the strongest Rossby wave sources occur in the Northern Hemisphere. Broadly speaking, the Rossby wave source over the Pacific is positive along the equatorward flank of the subtropical jet (Figure 12a) and negative on the poleward side of the subtropical jet, with the largest values lying over the

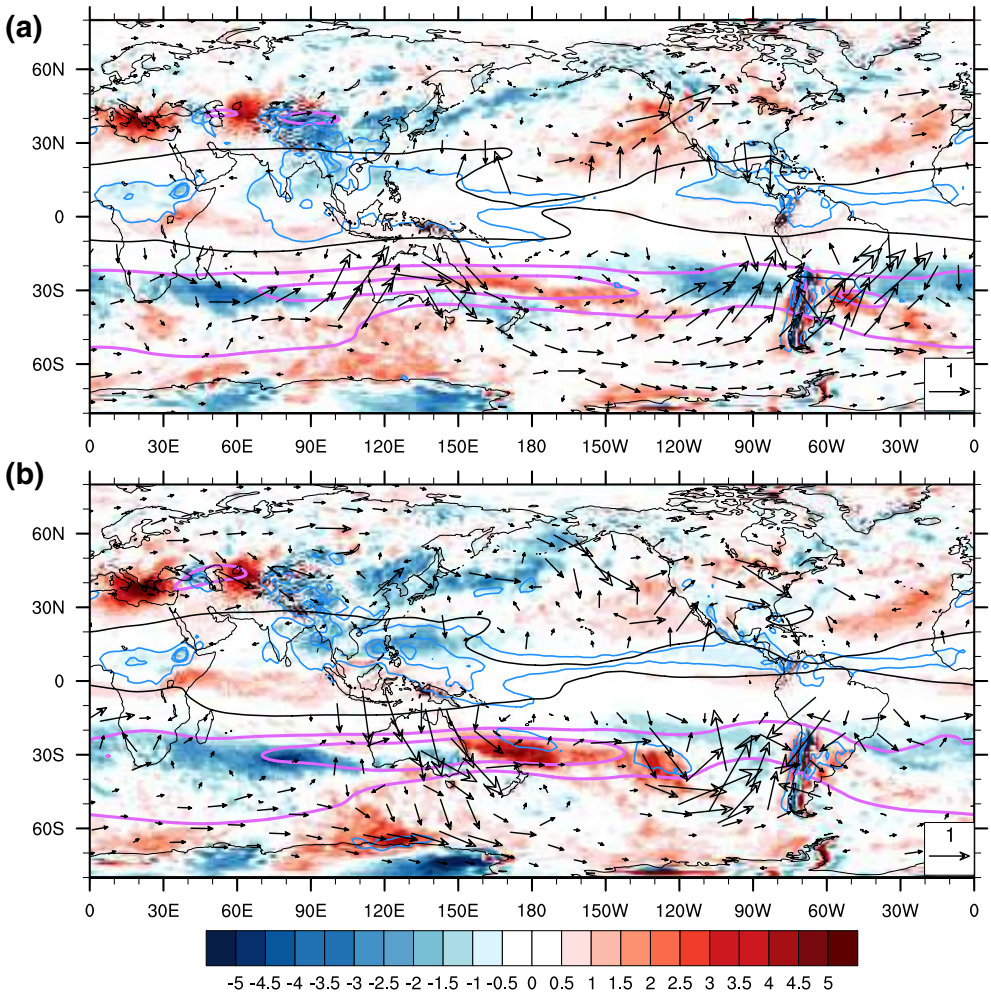

Figure 13. The same as Figure 12, but for JJA. JJA, June, July and August.

Central and Western Pacific. A similar pattern occurs in the North Atlantic. In the Southern Hemisphere, the Rossby wave source values are weaker than in the Northern Hemisphere. A positive Rossby wave source occurs between 40°S and 65°S East of the jet exit region located south of Australia.

In DJF in Phase 6 (Figure 12b), when the envelope of enhanced convection is located over the Maritime Continent, the areas of positive and negative Rossby wave source are roughly in the same region as during Phase 2 in both the Northern and Southern Hemisphere. The main differences are that the Rossby wave source is slightly stronger during Phase 6 than during Phase 2.

A similar observation can be made in JJA (Figure 13). The Rossby wave source is strongest in the winter hemisphere, but the differences in the distribution between Phases 2 and 6 are relatively small, aside from the magnitude in Phase 6 being somewhat larger than in Phase 2. One specific difference in JJA, however, is that positive values of the Rossby wave source start only at around 150°E compared to about 115°E during DJF. This displacement to the east is also apparent in the North Atlantic.

The surprising result here is that the mean (not the anomaly) Rossby wave source pattern is very similar regardless of whether the enhanced or suppressed phase of the MJO is located over the Maritime Continent, despite the subtropical jet responding differently in these phases. By examining the wave-activity flux, we will show that the source region for the midlatitude Rossby waves coincides with areas of enhanced upward mass flux, indicating that the Rossby waves form in relation to disturbances in the jet, caused by anomalous upper-level divergent flow of the enhanced or suppressed MJO convection.

5.2. Wave-Activity Flux

The arrows in Figures 12 and 13 represent the wave-activity flux. In the Northern Hemisphere, these arrows alternate in direction along the Eurasian jet, marking a stationary wave propagating along a waveguide. In Phase 2 (Figure 12a), the wave-activity flux originates roughly over India, whereas in Phase 6 (Figure 12b) the wave-activity flux vector originates over Southeast Asia. In both phases, there is a strong convergence of the wave-activity flux at the end of the jet near the west coast of North America.

In the Southern Hemisphere in Phase 2 (Figure 12a), there is enhanced wave-activity flux south of the region of enhanced convection. In Phase 6 (Figure 12b), the wave-activity flux emanates from the poleward extremities of the Maritime Continent near the critical line $c_p = 0$, and converges over southeastern Australia, which has been identified previously as a preferred region for Rossby wave breaking (e.g., Hitchman & Huesmann, 2007; Reeder et al., 2015), and in the southern Pacific.

In JJA in Phase 2 (Figure 13a), a prominent band of wave-activity flux emerges from northern Australia, follows a path to the southwest, before refracting toward the northeast, and converging over South America. A second, but less prominent, band emerges from southern Africa, before refracting and converging over northern Australia. In Phase 6 (Figure 13b), a pronounced wave-activity flux originates from the poleward extremities of the Maritime Continent, and follows a path to the high Southern Hemisphere latitudes. Again the wave-activity flux converges in the eastern Pacific. This region is not one of the Rossby wave breaking hot spots, but wave breaking does occur there (Hitchman & Huesmann, 2007).

McIntosh and Hendon (2018) have investigated Rossby wave trains in response to the Indian Ocean Dipole (IOD) and have shown that a strong subtropical jet in JJA inhibits the propagation of stationary waves from the tropics into the midlatitudes because the meridional gradient of the absolute vorticity goes to zero on the poleward side of the subtropical jet. The mean easterlies at upper levels in the tropics also provide an unfavorable environment for Rossby wave generation and propagation (Sardeshmukh & Hoskins, 1988). McIntosh and Hendon (2018) point out that two wave trains occur in the vicinity of Australia in JJA. One wave train is the result of enhanced convection associated with anomalous heating from the IOD and the associated enhanced upper-lever divergence. This evanescent wave train, however, cannot reach the midlatitudes due to the strong subtropical jet and is often refracted back into the tropics. The other wave train is located on the poleward side of the subtropical jet and is related to transient eddies. McIntosh and Hendon (2018) point out that in JJA the combination of both wave trains is typically seen in, for instance, geopotential height anomaly plots. They further argue that in austral spring, when the subtropical jet weakens, Rossby waves can propagate from the subtropics into the midlatitude and that these Rossby waves are forced by the upper-level anomalous divergent wind. The waves trains described in McIntosh and Hendon (2018) for the positive phase of the IOD, where convection is enhanced in the western Indian Ocean and suppressed in the eastern Indian Ocean, emanate from the western Indian Ocean. In contrast, the wave trains in Figure 13 emerge from over South Africa and north of Australia in MJO Phases 2 and 6.

Figures 12 and 13 show that the wave-activity flux vectors emerge poleward of the critical line $c_p = 0$ and poleward of the regions of enhanced upward mass flux. These Rossby waves are generated in the midlatitude westerlies and are a direct result of disturbances to the jet, which themselves are caused by changes to the local Hadley circulation as a result of the passing MJO.

5.3. Rossby Wave Source and Wave-Activity Flux Anomalies

To further support our conclusion from the previous sections, Figures 14 and 15 show the anomalies of the Rossby wave source and the wave-activity flux from the seasonal mean between 1979 and 2009. The stipples indicate regions where the anomalies are not statistically significant at the 95% confidence level. In DJF in Phase 2 of the MJO, a negative Rossby wave source anomaly is located over Asia and a positive anomaly over most of the North Pacific. A positive Rossby wave source anomaly occurs over the Indian Ocean in the Southern Hemisphere. In the Southwest Pacific the Rossby wave source anomaly is mainly negative. In Phase 6, the signal is almost reversed with a positive anomaly over Asia, a negative anomaly over the Northwest Pacific, a negative anomaly over the Southern Indian Ocean and a positive anomaly over the Western South Pacific.

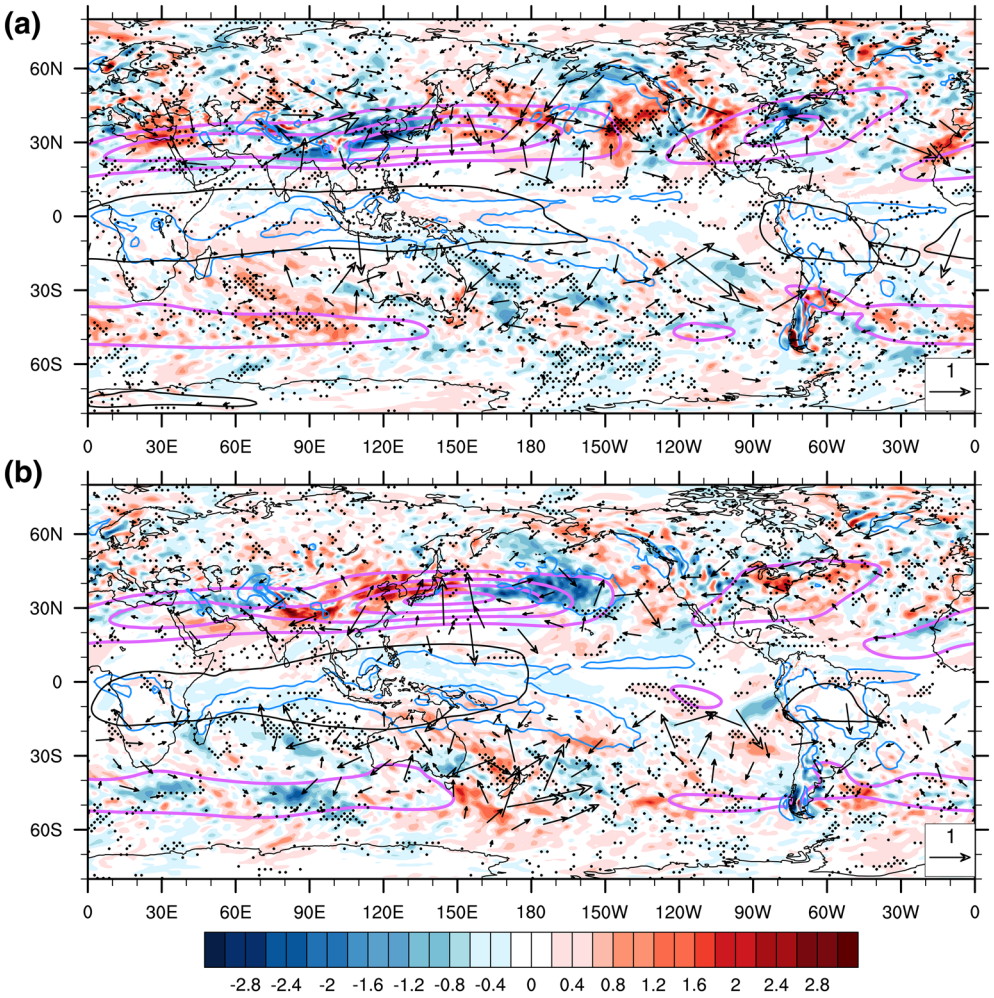

Figure 14. The anomalous Rossby wave source (shaded, 10^{-10} s^{-1}) and the anomalous wave-activity flux vector (arrows) at 200 hPa averaged over MJO phases (a) 2 and (b) 6 in DJF. The black contour displays the wave phase speed $C_p = 0$. The purple contours show the 200-hPa total windspeed greater than 30 $m\,s^{-1}$ in intervals of 15 $m\,s^{-1}$. The blue contour shows the meridional mass flux at 500 hPa greater than 0.002 $kg\,m^{-2}\,s^{-1}$ in intervals of 0.004 $kg\,m^{-2}\,s^{-1}$. The black stipples indicate regions where the Rossby wave source anomalies are not statistically different from the mean between 1979 and 2009 at the 95% confidence level. MJO, Madden-Julian Oscillation.

A similar behavior can be observed during the Southern Hemisphere winter (Figure 15). In JJA in MJO Phase 2 when the convection is located over the Indian Ocean, there is a positive anomaly located in the Southern Indian Ocean and a largely negative anomaly in the Southern West Pacific. In Phase 6, the signal is reversed and the positive Rossby wave source anomaly is located east of Australia near the jet core. The anomalies are weaker in the Northern Hemisphere, where they have the opposite sign. The Rossby wave source anomaly is largely positive over the North Pacific during MJO Phase 2 and largely negative in MJO phase 6.

The largest anomalies in the wave-activity flux overlap with the largest wave-activity flux vectors in Figures 12 and 13 and show that this anomalous wave activity is a result of the disturbances of the subtropical jet due to the MJO convection.

5.4. Interaction Between Midlatitude Rossby Waves and the Subtropical Jet

An alternative way to quantify the interaction between the subtropical jet and the midlatitude Rossby waves is to calculate the advection of the potential vorticity (PV) by the divergent part of the wind $\mathbf{u}_\chi$ on the 350-K surface following O'Brien and Reeder (2017):

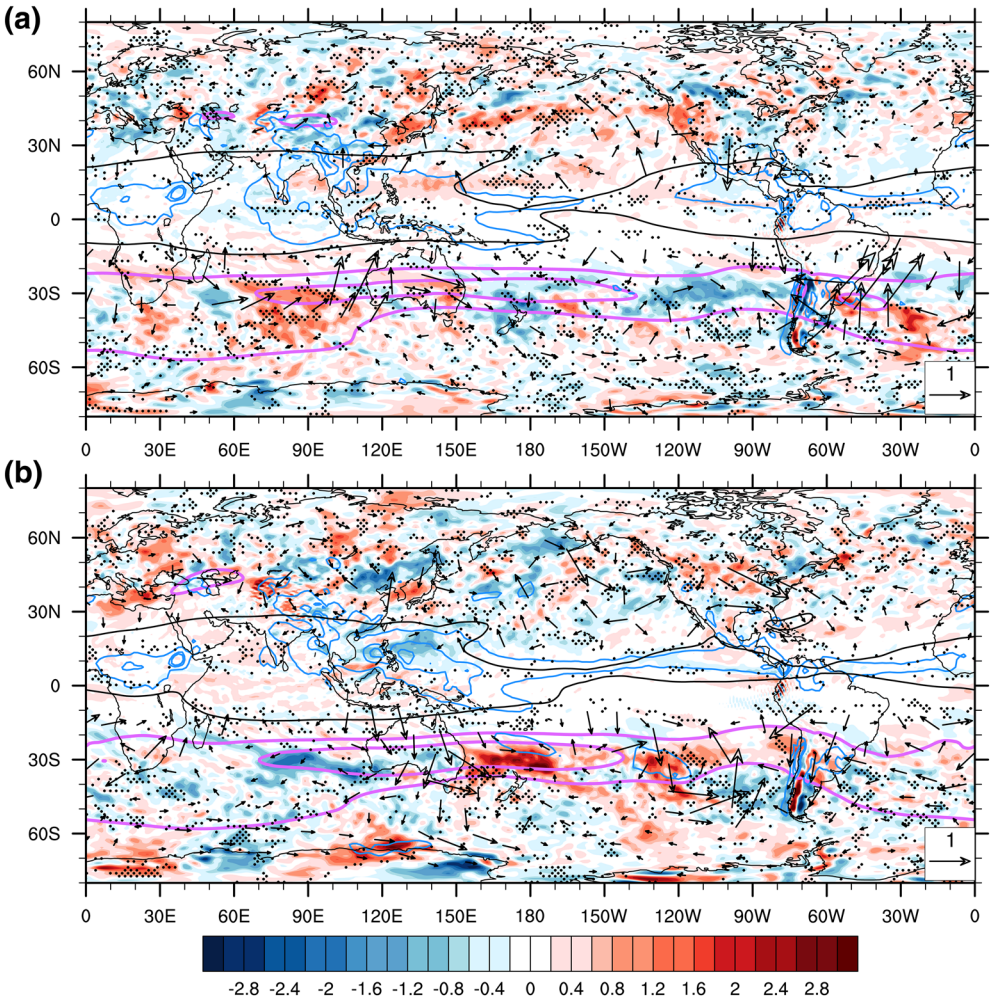

Figure 15. The same as Figure 14, but for JJA. JJA, June, July and August.

$$I = -\mathbf{u}_{\chi} \cdot \nabla PV. \tag{6}$$

The diagnostic I identifies where a disturbance interacts strongly with the jet, that is, where it displaces the jet. Such regions are not necessarily the source of the waves. O'Brien and Reeder (2017) have pointed out that I represents the deformation of the PV contours by the divergent part of the wind and can be interpreted as the local forcing of the barotropic Rossby wave equation in isentropic coordinates. The Rossby wave source S on the other hand represents the forcing of the barotropic vorticity equation in pressure coordinates. Regions of upper-level convergence on the equatorward side of the jet are associated with positive I, and regions of upper-level divergence on the equatorward side of the jet with negative I.

The anomalous advection of the PV by the divergent part of the wind at 350 K is shown for MJO phases 2 and 6 in DJF and JJA in Figures 16 and 17. In DJF in Phase 2 there is a positive anomaly of PV advection by the divergent part of the wind located roughly over the Arabian Peninsular and North India and a negative anomaly between 30°S and 60°S in the Southern Indian Ocean. A negative anomaly is located over the Northwestern Pacific and a positive anomaly over Eastern Australia and the Southwestern Pacific. The anomaly pattern in Phase 6 is the inverse of that in Phase 2. In line with O'Brien and Reeder (2017), positive I is associated with southerly divergent flow on the equatorward side of the jet and negative I with northerly divergent flow.

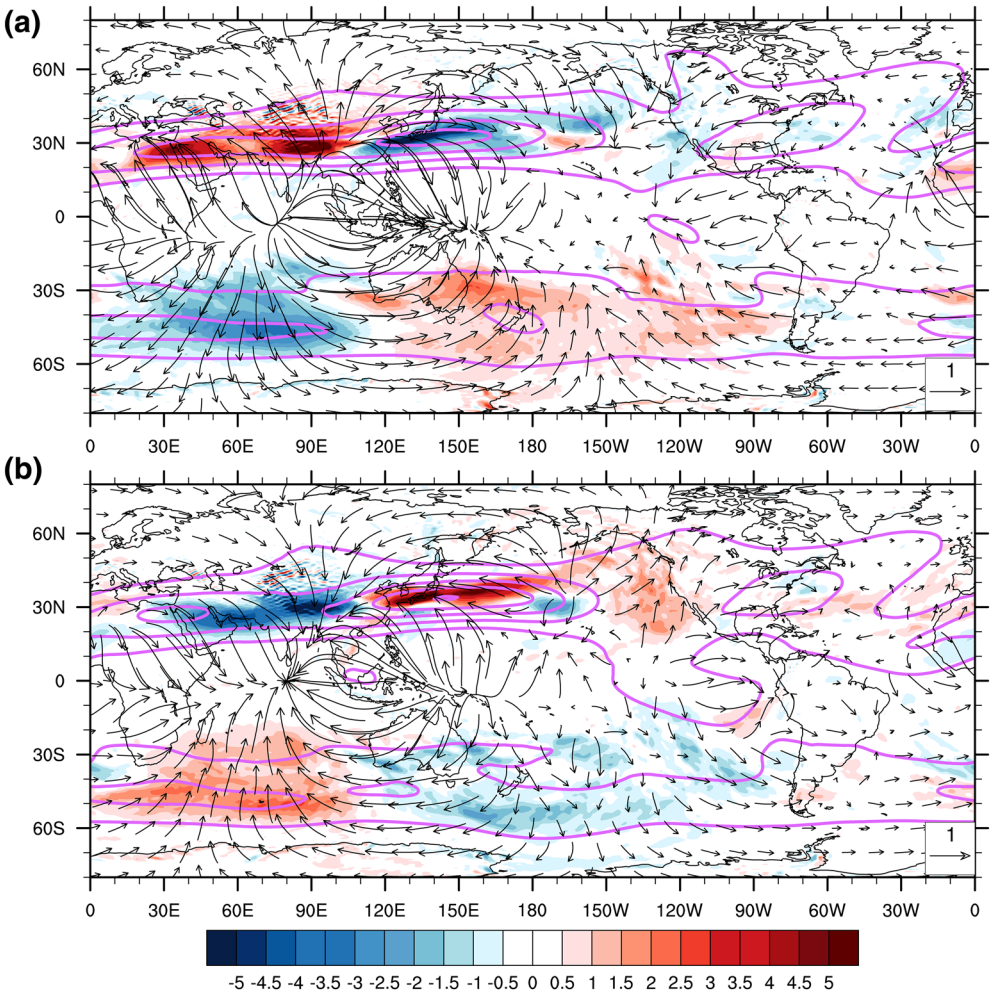

Figure 16. The anomalous advection of PV by the divergent part of the wind (shaded, PVU s^{-1}) and the anomalous divergent wind (arrows, $m\,s^{-1}$) at 350 K for MJO phases (a) 2 and (b) 6 in DJF. The purple contours show the 350-K total windspeed greater than 20 $m\,s^{-1}$ in intervals of 15 $m\,s^{-1}$. PV, potential vorticity; MJO, Madden-Julian Oscillation; December, January, February.

The anomaly patterns in PV advection are similar to those for the Rossby wave source in Figure 12, except they are much less noisy. The anomalies in PV advection in DJF and JJA (Figure 17) are similar, too. The anomalies are largest close to the jet axis and are stronger in the winter hemisphere than in the summer hemisphere.

O'Brien and Reeder (2017) have argued also that the anomalous divergent part of the wind in the tropics and subtropics leads to the advection of absolute and PV, which in turn leads to the formation of Rossby waves.

Our results are in agreement with those found in Lukens et al. (2017). For the Northern Hemisphere Lukens et al. (2017) have shown that the divergent outflow from the convection associated with the MJO over the western tropical Pacific is the main reason for the impact of the MJO on the midlatitudes in all MJO phases. They further showed that during Phases, 1, 2, 3, 7 the anomalous divergent winds advect absolute vorticity in the subtropics and, in combination with the horizontal convergence in the tropics, this leads to the formation of a cyclonic vorticity anomaly over southeast Asia. This cyclonic anomaly is then advected eastwards toward the central Pacific. In Phases 4, 5, 6, and 7, Lukens et al. (2017) observed the formation of an anticyclonic anomaly over Southeast Asia. The authors also pointed out that once the vorticity anomaly reached the jet exit region it was no longer trapped and could propagate poleward.

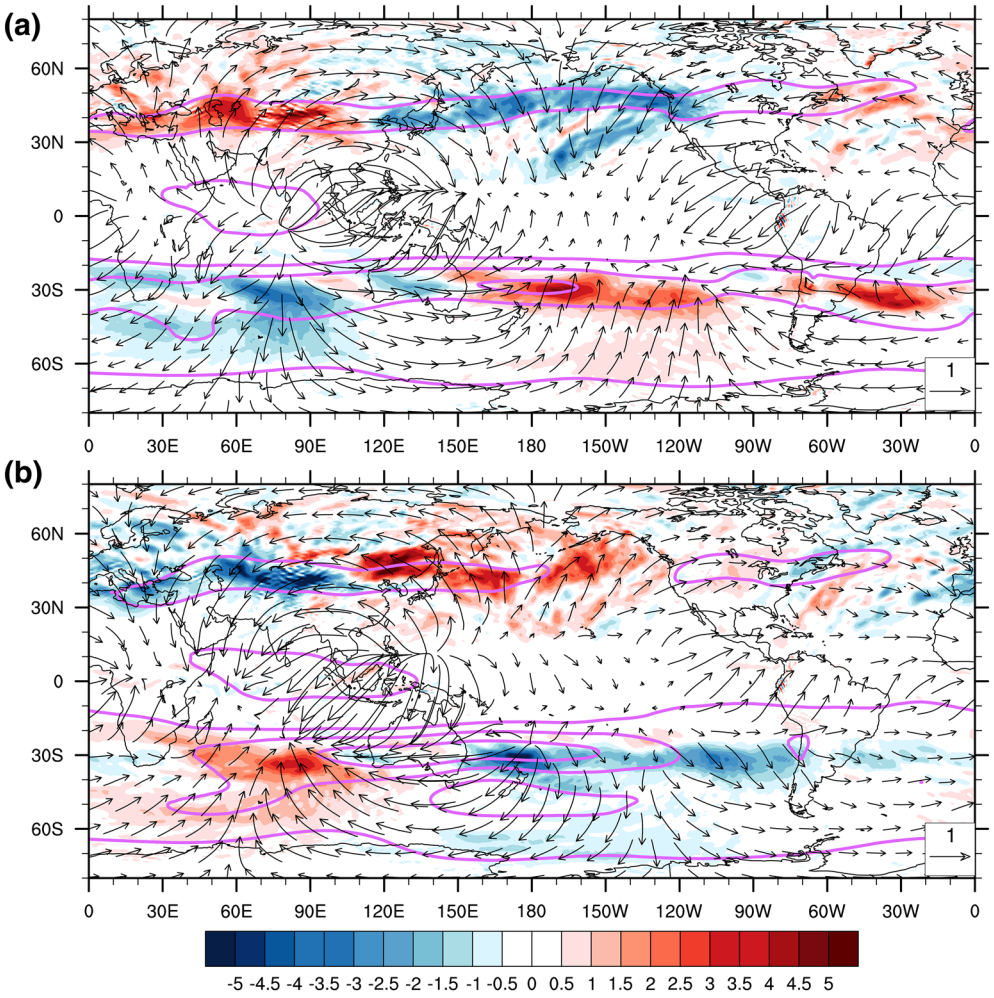

Figure 17. The same as Figure 16, but for JJA. JJA, June, July and August.

We have shown that the anomalous upper-level outflow of regional Hadley circulations disturbs in the subtropical jet and that these disturbances are the source for midlatitude Rossby waves. The wave-activity flux shows the propagation of these waves along the midlatitude storm tracks.

5.5. Rossby Wave Propagation in the Midlatitudes

The link between changes in the subtropical jet, due to enhanced and suppressed MJO convection and therefore a strengthened or weakened local Hadley circulation, and the downstream propagation of the midlatitude Rossby waves is made even more apparent when looking at the midlatitude wave signal in the Hovmöller plots in Figures 18 and 19. The zonal mass flux anomalies (based on m_λ) and the wave-activity flux are meridionally averaged over 40°N–60°N and 40°S–60°S. We show the anomaly of the zonal mass flux from the 31-year mean in each MJO phase as they display the anomalies in the zonal direction, that is, the direction of the midlatitude waves, distinctly. Additionally, the wind speed anomaly from the 31-year wind speed mean averaged over 20°N–40°N and 20°S–40°S is shown in contours. The averaging band for the wind speed is chosen to include the maximum of the jet, so as to link the changes in the jet to the stationary Rossby wave pattern. The MJO phase is shown on the abscissa and the ordinate shows the longitude. The fields have been interpolated for plotting to give a sense of the continuity in time.

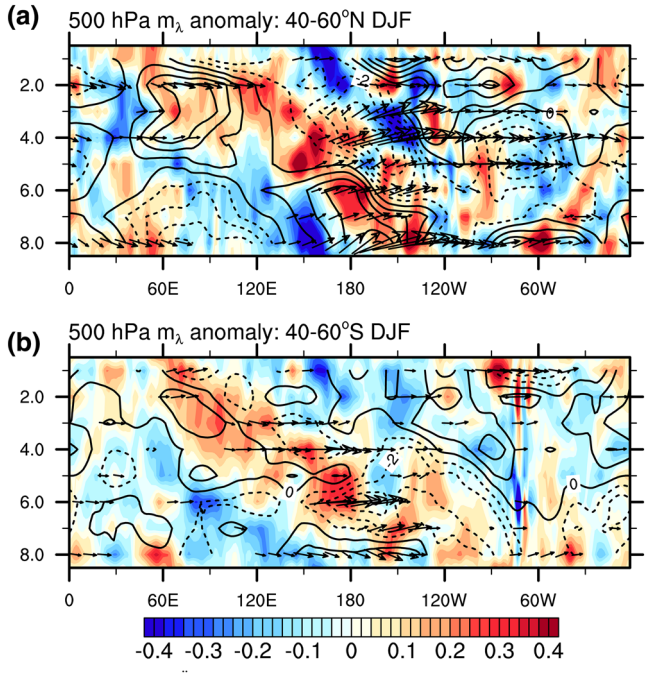

Figure 18. Hovmöller plots showing the anomalous zonal mass flux (shaded, kg m^{-2} s^{-1}) relative to the 31-year mean in each MJO phase, as well as the wave-activity flux vector (arrows) in DJF for (a) the Northern Hemisphere and (b) the Southern Hemisphere. The black contours show the wind speed anomalies. Solid contours indicate positive values, and dashed lines negative values. The contour interval is 1 m s^{-1}. The zonal mass flux and the wave-activity flux are meridionally averaged between 40°N and 60°N and 40°S–60°S. The wind speed anomalies are calculated in the bands 20°N–40°N and 20°S–40°S. The vectors are scaled by the aspect ratio of the plots, which means the direction they are pointing in is correct in the Earth relevant sense, but the absolute magnitude has no physical meaning. The relative magnitude of the vectors to each other is maintained, and small values are excluded for clarity. The abscissa shows the MJO phases 1 to 8 and the ordinate shows the longitude. MJO, Madden-Julian Oscillation; DJF, December, January, February.

Broadly speaking, in DJF and JJA the regions of upward and downward mass flux are relatively similar. Bands of upward and downward mass flux, which represent a quasi-stationary wave pattern, propagate eastward with the MJO as the region of enhanced convection moves from East Africa to the Central Pacific. The eastward propagation of the Rossby waves is illustrated by the wave-activity flux vectors.

In the Northern Hemisphere in DJF (Figure 18a), the wave-activity flux has a northeastward direction and is strongest over the Pacific Ocean (roughly between 160°E and 120°W) in Phases 3–8. The wave-activity flux is largest in magnitude in Phases 3, 4, and 8. In Phases 4 and 5 the wave-activity flux vector is directed to the east and the magnitude is also relatively large over North America. The wave-activity flux is, in general, weaker in the Southern Hemisphere (Figure 18b) than the Northern Hemisphere, and is also largest over the Pacific Ocean. Moreover, in both hemispheres, the wind speed anomalies also propagate from west to east with the MJO phase. The wind speed anomalies are largest over the Maritime Continent in all MJO phases and coincide with the largest wave-activity flux vectors.

The bands of anomalous upward and downward mass flux are less coherent in JJA (Figure 19a, b) than in DJF, particularly in the Southern Hemisphere. In the Northern Hemisphere, the largest wave-activity flux occurs in Phases 3 and 8 over the Pacific Ocean. In the Southern Hemisphere, the largest wave-activity flux occurs in Phase 6 and 7. Once again, positive and negative wind speed anomalies move from west to east, with the largest anomalies in the winter hemisphere.

In summary, the anomalous upper-level divergence (convergence) of the region of enhanced (suppressed) convection associated with the MJO leads to changes in the speed and location of the subtropical jet. These disturbances in the jet, along with the advection of absolute vorticity, lead to the formation of a mid-latitude quasi-stationary wave pattern, which changes the propagation characteristics of the Rossby waves.

6. Summary and Conclusions

We set out to investigate: (i) how the local Hadley and Walker circulations change in each phase of the MJO; and (ii) how the propagation of the envelope of enhanced and suppressed convection affects the poleward extent of the local Hadley circulations and the strength and position of the subtropical jet. We addressed these questions by objectively decomposing the vertical mass flux into zonal and meridional components following the ψ-vector method of Keyser et al. (1989) modiefied by Schwendike et al. (2014). We applied this method to 31 years of ERAI reanalysis data. The advantage of the ψ-vector method is that it allows us to study local Hadley and Walker circulations and their link to the MJO in an unambiguous way.

We have shown, for the first time, that as the envelope of enhanced precipitation moves from Africa to the Central Pacific, the local Hadley circulation is enhanced by about 2 kg m^{-2} s^{-1}. The regional Walker circulation in the Pacific is weakened when the suppressed phase of MJO convection is located over the Maritime Continent, and doubles in strength when the active phase of MJO convection occurs over the Maritime Continent. The changes in both local Hadley and Walker circulations are of about the same magnitude. As the local Hadley circulation is climatologically larger than the local Walker circulation (Schwendike et al., 2014), the percentage change in the local Walker circulation is higher than in the local Hadley circulation.

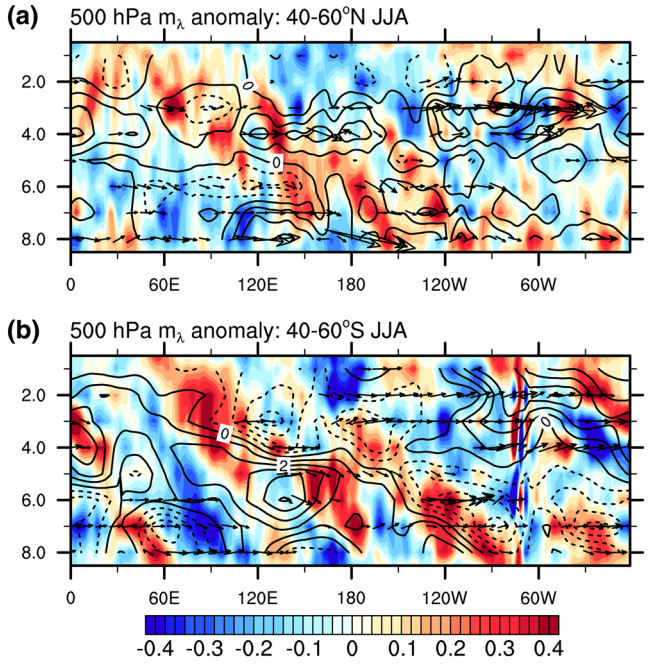

Figure 19. The same as Figure 18, but for JJA. JJA, June, July and August.

Due to the changes in the local Hadley and Walker circulations, the resulting anomalous upper-level divergence (convergence) affects the position and strength of the subtropical jet. The jet is strengthened in regions of upper-level divergence and is weakened in regions of upper-level convergence. Moore et al. (2010) noted that the jet maximum in the Pacific moves with the envelope of enhanced convection, similarly to our results. Over the Indian Ocean, the jet core is displaced farther poleward (equatorward) by the enhanced upper-level divergence (convergence). However, we also find that over India the jet is displaced northwards by about 3–5° and over the Southern Indian Ocean the jet is displaced southwards by about 1–3°. Over the Pacific Ocean, the position of the jet hardly changes.

Additionally, the jets over the Northwestern Pacific, the Southwestern Pacific and the North Atlantic have been characterized in each MJO Phase for the first time. For both jets in the Northwest and Southwest Pacific in winter, the peak jet core speed, the depth of the jet and the mass transport in the jet increase when the active phase of the MJO convection is located over the Maritime Continent. Simultaneously the width of the jet decreases. These four characteristics of the jet also change for the jet in the North Atlantic, but less coherently. This is probably because the anomalous outflow of the either strengthened or weakened local Hadley circulation does not directly reach the North Atlantic. During summer, as expected, the jets in all regions are weaker than in winter due to the weaker meridional temperature contrast, and the changes in jet characteristics are largest for the jet in the Northwest Pacific.

These changes in the strength and location of the jet associated with changes in the local Hadley circulation in different phases of the MJO, lead to disturbances in the jet, which result in quasi-stationary wave patterns that extend into the midlatitudes in both hemispheres and modify the propagation of midlatitude Rossby waves. This wave pattern is strongest in the winter hemisphere. The stationary Rossby wave response to the MJO has been pointed out by a number of previous studies (e.g., Hendon & Salby, 1994; Higgins & Mo, 1997; Kiladis & Weickmann, 1992; Knutson & Weickmann, 1987; Lukens et al., 2017; Matthews et al., 2004).

By calculating the Rossby wave source anomalies globally we have shown that Rossby waves form as a result of disturbances in the midlatitude jet due to either enhanced or suppressed convection over the Maritime Continent. The wave-activity flux vector shows how the Rossby waves then propagate away from the jet into the midlatitudes. The Rossby wave source calculations also show that Rossby waves are generated from both enhanced and suppressed convection in all MJO phases. The calculation of the anomalous advection of the PV by the divergent part of the wind shows regions of interaction between Rossby waves and the subtropical jet.

We have shown, for the first time, that the local Hadley and Walker circulations are regionally enhanced when they overlap with the convectively active phase of the MJO. We have also shown that the anomalous upper-level divergence (convergence) of the local Hadley circulation during enhanced (suppressed) phases of the MJO leads to a northwards shift of the subtropical jet maximum over the continents, and a shift of the jet maximum toward the region of enhanced MJO convection. These disturbances in the jet lead then to the formation of quasi-stationary midlatitude wave trains. This study supports the sometimes questioned view that the MJO plays an important role in the tropics, subtropics and midlatitudes in both hemispheres.

Data Availability Statement

The data used in this analysis were provided by the European Centre for Medium Range Weather Forecasts (http://data-portal.ecmwf.int/data/d/interim_daily/). The TRMM rainfall data were obtained from the National Aeronautics and Space Administration (NASA) and the Goddard Space Flight Centre (https://pmm.

nasa.gov/data-access/downloads/trmm). The RMM index data are available from http://www.bom.gov.au/climate/mjo. The SOI index data are available from http://www.bom.gov.au/climate/current/soi2.shtml.

Acknowledgments
The authors would like to thank Brian Hoskins for his helpful suggestions. They are grateful to Kay Shelton for her help with the bootstrapping method. They also thank the three anonymous reviewers for their helpful comments to significantly improve this manuscript.

References

Barry, R. G., & Carleton, A. M. (2001). *Synoptic and dynamic climatology*. London and New York: Routledge.
Berry, G. J., & Reeder, M. J. (2014). Objective identification of the intertropical convergence zone: Climatology and trends from the ERA-Interim. *Journal of Climate*, *27*, 1894–1909.
Berry, G. J., Reeder, M. J., & Jakob, C. (2011). A global climatology of atmospheric fronts. *Geophysical Research Letters*, *38*. https://doi.org/10.1029/2010GL046451
Berry, G. J., Thorncroft, C. D., & Hewson, T. (2007). African easterly waves during 2004 - Analysis using objective techniques. *Monthly Weather Review*, *135*, 1251–1267.
Cassou, C. (2008). Intraseasonal interaction between the Madden-Julian Oscillation and the North Atlantic Oscillation. *Nature*, *455*, 523–527.
Dee, D. P., Uppala, S. M., Simmons, A. J., Berrisford, P., Poli, P., Kobayashi, S., et al. (2011). The ERA-Interim reanalysis: Configuration and performance of the data assimilation system. *Quarterly Journal of the Royal Meteorological Society*, *137*, 553–597.
Hall, N. M. J., Le, H. H., & Leroux, S. (2020). The extratropical response to a developing MJO: Forecast and climate simulations with the DREAM model. *Climate Dynamics*, *55*, 813–829.
Hartmann, D. (1994). *Global physical climatology*, San Diego: Academic Press.
Hendon, H. H., & Salby, M. L. (1994). The life cycle of the Madden-Julian oscillation. *Journal of the Atmospheric Sciences*, *51*, 1751–1758.
Hesterberg, T., Monaghan, S., Moore, D. S., Clipson, A., & Epstein, R. (2003). *Bootstrap methods and permutation tests*. W. H. Freeman and Company.
Higgins, R. M., & Mo, K. C. (1997). Persistent North Pacific circulation anomalies and the tropical intraseasonal oscillation. *Journal of Climate*, *10*, 223–244.
Hitchman, M. H., & Huesmann, A. S. (2007). A seasonal climatology of Rossby wave breaking in the 320-2000-K layer. *Journal of the Atmospheric Sciences*, *64*, 1922–1940.
Huffman, G. J., Adler, R. F., Bolvin, D. T., & Nelkin, E. J. (2010). The TRMM multi-satellite precipitation analysis (TMPA). In M. Gebremichael, & F. Hossain (Eds.), *Satellite rainfall applications for surface hydrology* (pp. 3–22). Springer.
Julian, P. R., & Chervin, R. M. (1978). A study of the Southern Oscillation and the Walker circulation phenomenon. *Monthly Weather Review*, *106*, 1433–1451.
Keyser, D., Schmidt, B. D., & Duffy, D. G. (1989). A technique for representing three-dimensional vertical circulations in baroclinic disturbance. *Monthly Weather Review*, *117*, 2463–2494.
Kiladis, G. N., & Weickmann, K. M. (1992). Circulation anomalies associated with tropical convection during northern winter. *Monthly Weather Review*, *120*, 1900–1923.
Knutson, T. R., & Weickmann, K. L. (1987). 30-60 day atmospheric oscillations: Composite life cycles of convection and circulation anomalies. *Monthly Weather Review*, *115*, 1407–1436.
Lin, H., Brunet, G., & Derome, J. (2009). An observed connection between the North Atlantic Oscillation and the Madden-Julian Oscillation. *Journal of Climate*, *22*, 364–380.
Lukens, K. E., Feldstein, S. B., Yoo, C., & Lee, S. (2017). The dynamics of the extratropical response to Madden-Julian oscillation convection. *Quarterly Journal of the Royal Meteorological Society*, *143*, 1095–1106.
L'Heureux, M. L., & Higgins, R. W. (2008). Boreal winter links between the Madden-Julian oscillation and the Arctic oscillation. *Journal of Climate*, *21*, 3040–3050.
L'Heureux, M. L., Lee, S., & Lyon, B., (2013). Recent multidecadal strengthening of the Walker circulation across the tropical Pacific, *Nature Climate*, *3*, 571–576. https://doi.org/10.1038/NCLIMATE1840
Madden, R. A., & Julian, P. (1972). Description of global scale circulation cells in the tropics with a 40-50 day period. *Journal of the Atmospheric Sciences*, *29*, 1109–1123.
Madden, R. A., & Julian, P. (1994). Observations of the 40-50 day tropical oscillation - A review. *Monthly Weather Review*, *122*, 814–837.
Matthews, A. J., Hoskins, B. J., & Masutani, M. (2004). The global response to tropical heating in the Madden-Julian oscillation during the northern winter. *Quarterly Journal of the Royal Meteorological Society*, *130*, 1991–2011.
Matthews, A. J., Hoskins, B. J., Slingo, J. M., & Blackburn, M. (1996). Development of convection along the SPCZ within a Madden-Julian oscillation. *Quarterly Journal of the Royal Meteorological Society*, *122*, 669–688.
Matthews, A. J., & Kiladis, G. N. (1999). The tropical-extratropical interaction between high-frequency transients and the Madden-Julian Oscillation. *Monthly Weather Review*, *127*, 661–688.
McIntosh, P. C., & Hendon, H. H. (2018). Understanding Rossby wave trains forced by the Indian Ocean Dipole. *Climate Dynamics*, *50*, 2783–2798.
Moore, R. W., Martius, O., & Spengler, T. (2010). The modulation of the subtropical and extratropical atmosphere in the Pacific basin in response to the Madden-Julian oscillation. *Monthly Weather Review*, *138*, 2761–2779.
Mori, M., & Watanabe, M. (2008). The growth and triggering mechanisms of the PNA: A MJO-PNA coherence. *Journal of the Meteorological Society of Japan*, *86*, 213–236.
O'Brien, L., & Reeder, M. J. (2017). Southern Hemisphere summertime Rossby waves and weather in the Australian region. *Quarterly Journal of the Royal Meteorological Society*, *143*, 2374–2388.
Power, S., & Smith, I. (2007). Weakening of the Walker Circulation and apparent dominance of El-Nino both reach record levels, but has ENSO really changed? *Geophysical Research Letters*, *34*, 854. https://doi.org/10.1029/2007GL030
Reeder, M. J., Spengler, T., & Musgrave, R. (2015). Rossby waves, extreme fronts, and wildfires in southeastern Australia. *Geophysical Research Letters*, *42*, 2015–2023.
Renwick, J. A., & Revell, M. J. (1999). Blocking over the South Pacific and Rossby wave propagation. *Monthly Weather Review*, *127*, 2233–2247.
Sardeshmukh, P. D., & Hoskins, B. J. (1988). The generation of global rotational flow by steady idealized tropical divergence. *Journal of the Atmospheric Sciences*, *45*, 79–96.

Schwendike, J., Berry, G. J., Reeder, M. J., Govekar, C. J. P., & Wardle, R. (2015). Trends in the local Hadley and Walker circulations. *Journal of Geophysical Research: Atmospheres*, *120*, 7599–7618. https://doi.org/10.1002/2014JD022652

Schwendike, J., Govekar, P., Reeder, M. J., Wardle, R., Berry, G. J., & Jakob, C. (2014). Local partitioning of the overturning circulation in the tropics and the connection to the Hadley and Walker circulations. *Journal of Geophysical Research: Atmospheres*, *119*, 1322–1339. https://doi.org/10.1002/2013JD020742

Shao, X., Song, J., & Li, S. (2019). The lagged connection of the positive NAO with the MJO Phase 3 in a simplified atmospheric model. *Climate Dynamics*, *135*, 1091–1103.

Simmons, A., Uppala, S., Dee, D., & Kobayashi, S. (2011). New ECMWF reanalysis products from 1989 onwards. *ECMWF Newsletter*, *110*, 26–35.

Takaya, K., & Nakamura, H. (2001). A formulation of a phase-independent wave-activity flux for stationary and migratory quasigeostrophic eddies on a zonally varying basic flow. *Journal of the Atmospheric Sciences*, *58*, 608–627.

Tokinaga, H., Xie, S.-P., Deser, C., Kosaka, Y., & Okumura, Y. M. (2012). Slowdown of the Walker circulation driven by tropical Indo-Pacific warming. *Nature*, *491*, 439–443.

Trenberth, K., & Stepaniak, D. (2003). Seamless poleward atmospheric energy transports and implications for the Hadley circulation. *Journal of Climate*, *16*, 3706–3722.

Vecchi, G., Soden, B., Wittenberg, A., Held, I., Leetmaa, A., & Harrison, M. (2006). Weakening of tropical Pacific atmospheric circulation due to anthropogenic forcing. *Nature*, *441*, 73–76.

Wheeler, M. C., & Hendon, H. H. (2004). An all-season real-time multivariate MJO index: Development of an index for monitoring and prediction. *Monthly Weather Review*, *132*, 1917–1932.

Zhang, C. (2005). Madden-Julian Oscillation. *Reviews of Geophysics*, *43*. https://doi.org/10.1029/2004RG000158

Zhang, C. (2013). Madden-Julian Oscillation - Bridging weather and climate. *Bulletin of the American Meteorological Society*, *94*, 1849–1870.

Zheng, C., & Chang, E. K. M. (2019). The role of MJO propagation, lifetime, and intensity on modulating the temporal evolution of the MJO extratropical response. *Journal of Geophysical Research: Atmospheres*, *124*, 5352–5378. https://doi.org/10.1029/2019JD030258

Zurita-Gotor, P. (2019). The role of the divergent circulation for large-scale eddy momentum transport in the tropics. Part I: Observations. *Journal of the Atmospheric Sciences*, *76*, 1125–1144.